Monthly Notices
of the
ROYAL ASTRONOMICAL SOCIETY

Mon. Not. R. Astron. Soc. **417,** 863–881 (2011) doi:10.1111/j.1365-2966.2011.19137.x

The ATLAS^{3D} project – IX. The merger origin of a fast- and a slow-rotating early-type galaxy revealed with deep optical imaging: first results

Pierre-Alain Duc,[1⋆] Jean-Charles Cuillandre,[2] Paolo Serra,[3] Leo Michel-Dansac,[4] Etienne Ferriere,[1] Katherine Alatalo,[5] Leo Blitz,[5] Maxime Bois,[4,6] Frédéric Bournaud,[1] Martin Bureau,[7] Michele Cappellari,[7] Roger L. Davies,[7] Timothy A. Davis,[7] P. T. de Zeeuw,[6,8] Eric Emsellem,[4,6] Sadegh Khochfar,[9] Davor Krajnović,[6] Harald Kuntschner,[10] Pierre-Yves Lablanche,[4] Richard M. McDermid,[11] Raffaella Morganti,[3,12] Thorsten Naab,[13] Tom Oosterloo,[3,12] Marc Sarzi,[14] Nicholas Scott,[7] Anne-Marie Weijmans[15]† and Lisa M. Young[16]

[1]*Laboratoire AIM Paris-Saclay, CEA/IRFU/SAp, CNRS/INSU, Université Paris Diderot, 91191 Gif-sur-Yvette Cedex, France*
[2]*Canada–France–Hawaii Telescope Corporation, 65-1238 Mamalahoa Hwy., Kamuela, HI 96743, USA*
[3]*Netherlands Institute for Radio Astronomy (ASTRON), Postbus 2, 7990 AA Dwingeloo, the Netherlands*
[4]*Centre de Recherche Astrophysique de Lyon, Université Lyon 1, Observatoire de Lyon, Ecole Normale Supérieure de Lyon, CNRS, UMR 5574, 9 avenue Charles André, F-69230 Saint-Genis Laval, France*
[5]*Department of Astronomy, Campbell Hall, University of California, Berkeley, CA 94720, USA*
[6]*European Southern Observatory, Karl-Schwarzschild-Str. 2, 85748 Garching, Germany*
[7]*Sub-Department of Astrophysics, Department of Physics, University of Oxford, Denys Wilkinson Building, Keble Road, Oxford OX1 3RH*
[8]*Sterrewacht Leiden, Leiden University, Postbus 9513, 2300 RA Leiden, the Netherlands*
[9]*Max Planck Institut für extraterrestrische Physik, PO Box 1312, D-85478 Garching, Germany*
[10]*Space Telescope European Coordinating Facility, European Southern Observatory, Karl-Schwarzschild-Str. 2, 85748 Garching, Germany*
[11]*Gemini Observatory, Northern Operations Centre, 670 N. A'ohoku Place, Hilo, HI 96720, USA*
[12]*Kapteyn Astronomical Institute, University of Groningen, Postbus 800, 9700 AV Groningen, the Netherlands*
[13]*Max-Planck-Institut für Astrophysik, Karl-Schwarzschild-Str. 1, 85741 Garching, Germany*
[14]*Centre for Astrophysics Research, University of Hertfordshire, Hatfield, Herts AL1 9AB*
[15]*Dunlap Institute for Astronomy & Astrophysics, University of Toronto, 50 St George Street, Toronto, ON M5S 3H4, Canada*
[16]*Physics Department, New Mexico Institute of Mining and Technology, Socorro, NM 87801, USA*

Accepted 2011 May 25. Received 2011 May 25; in original form 2011 January 27

ABSTRACT

The mass assembly of galaxies leaves imprints in their outskirts, such as shells and tidal tails. The frequency and properties of such fine structures depend on the main acting mechanisms – secular evolution, minor or major mergers – and on the age of the last substantial accretion event. We use this to constrain the mass assembly history of two apparently relaxed nearby early-type galaxies (ETGs) selected from the ATLAS^{3D} sample, NGC 680 and 5557. Our ultra-deep optical images obtained with MegaCam on the Canada–France–Hawaii Telescope reach 29 mag arcsec^{-2} in the *g* band. They reveal very low surface brightness (LSB) filamentary structures around these ellipticals. Among them, a gigantic 160 kpc long, narrow, tail east of NGC 5557 hosts three gas-rich star-forming objects, previously detected in H I with the Westerbork Synthesis Radio Telescope and in UV with *GALEX*. NGC 680 exhibits two major diffuse plumes apparently connected to extended H I tails, as well as a series of arcs and shells. Comparing the outer stellar and gaseous morphology of the two ellipticals with that predicted from models of colliding galaxies, we argue that the LSB features are tidal debris and that

⋆E-mail: paduc@cea.fr
†Dunlap Fellow.

each of these two ETGs was assembled during a relatively recent, major wet merger, which most likely occurred after the redshift $z \simeq 0.5$ epoch. Had these mergers been older, the tidal features should have already fallen back or be destroyed by more recent accretion events. However, the absence of molecular gas and of a prominent young stellar population in the core region of the galaxies indicates that the merger is at least 1–2 Gyr old: the memory of any merger-triggered nuclear starburst has indeed been lost. The star-forming objects found towards the collisional debris of NGC 5557 are then likely tidal dwarf galaxies. Such recycled galaxies here appear to be long-lived and continue to form stars while any star formation activity has stopped in their parent galaxy. The inner kinematics of NGC 680 is typical for fast rotators which make the bulk of nearby ETGs in the ATLAS^{3D} sample. On the other hand, NGC 5557 belongs to the poorly populated class of massive, round, slow rotators that are predicted by semi-analytic models and cosmological simulations to be the end-product of a complex mass accretion history, involving ancient major mergers and more recent minor mergers. Our observations suggest that under specific circumstances a single binary merger may dominate the formation history of such objects and thus that at least some massive ETGs may form at relatively low redshift. Whether the two galaxies studied here are representative of their own sub-class of ETGs is still an open question that will be addressed by an on-going deep optical survey of ATLAS^{3D} galaxies.

Key words: galaxies: elliptical and lenticular, cD – galaxies: formation – galaxies: individual: NGC 5557 – galaxies: individual: NGC 680 – galaxies: interactions.

1 INTRODUCTION

According to standard hierarchical cosmological models, the formation of galaxies is a gradual process based on the assembly of building blocks making their mass, and on the accretion of gas making their stars. The details of this scenario are, however, still under active discussion. The debate has been specifically hot for the population of early-type galaxies (ETGs), since, being the most massive systems, they are believed to be the end product of the mass assembly process. Since the seminal simulation by Toomre (1977) of a spiral–spiral collision and follow-up works (e.g. Negroponte & White 1983) showing that the merger remnant had a de Vaucouleurs profile (e.g. Hibbard & Yun 1999), much attention has been given to the merger scenario for the formation of ETGs. However, the luminosity profile is by far not the only parameter that characterizes galaxies. The SAURON (de Zeeuw et al. 2002) and ATLAS^{3D} projects (Cappellari et al. 2011a, hereafter Paper I) have recently provided a wealth of observational data on nearby ETGs of particular use for constraining their nature. In particular, the study of the inner stellar kinematics enabled by integral field spectroscopy put the attention on some little-known properties of ETGs: the large majority (80–85 per cent) of ETGs rotate; a fraction of ETGs, especially among the slow-rotating systems, show intriguing features, such as Kinematically Distinct Components (KDCs), including counter-rotating cores (Krajnović et al. 2011, hereafter Paper II). This suggests that although ETGs globally follow common scaling relations, they might in fact constitute different families of objects, with different histories for their mass assembly. Complementary to the observational efforts, various types of numerical simulations have been carried out to reproduce the photometric and kinematical properties of ETGs: binary major and minor mergers (among the most recent ones; Jesseit et al. 2009; Johansson, Naab & Burkert 2009; Di Matteo et al. 2009; Bois et al. 2010; Hoffman et al. 2010), series of major mergers (Weil & Hernquist 1996), minor mergers (e.g. Bournaud, Jog & Combes 2007), multiple collisions following hierarchical structure formation scenarios (e.g. Naab, Khochfar & Burkert 2006; Burkert et al. 2008) or cosmological simulations with zoom-in techniques (e.g. Martig et al. 2009). Most of these models successfully form the fast rotators that dominate the bulk of the ETG population. The formation of the slow rotators with single binary mergers turns out to be more difficult (Bois et al. 2011, hereafter Paper VI). Producing the massive, round, ones typically located in groups and clusters seems to require a complex mass assembly history that was initiated at high redshift by a major merger (Khochfar et al. 2011, hereafter Paper VIII).

Characterizing and dating the mergers that contributed to the mass assembly of galaxies appear thus as fundamental. Among the most valuable and convenient tracers of mergers are the fine structures around galaxies: shells, rings, plumes and tails. Indeed, depending on whether massive galaxies were formed through a monolithic collapse, rapid cold-gas accretion followed by violent disc instabilities, minor/major, gas-rich/gas-poor mergers, the ubiquity of collisional debris will go from none to significant. Furthermore, relics like tidal tails are transient structures with surviving ages varying between a few hundred Myr to a few Gyr, depending on their nature and location (Hibbard & Mihos 1995). Their observations thus provide a clock that can be calibrated using numerical simulations.

Collisional relics may be traced mapping their hydrogen gas with radio interferometers or imaging their stellar populations with optical cameras. Malin & Carter (1980) have used optical photographs of ellipticals and unsharp masking techniques to disclose concentric stellar shells around some massive ellipticals. These fine structures are generally interpreted as imprints of accretion and disruption of low-mass satellites. Schweizer et al. (1990) and Schweizer & Seitzer (1992) performed a more systematic survey of fine structures around ETGs, introducing a fine structure index Σ which basically characterizes the number of observed distinct features, such as ripples and jets. Unfortunately, collisional debris are generally faint, and those tracing most efficiently major mergers – the 50–100 kpc long tidal tails – have a surface brightness that is typically 24–26 mag arcsec^{-2} when young and below 27 mag arcsec^{-2} when getting older and fading. Their detection requires specific

observing conditions and techniques: for galaxies that are resolved in stars, star counts allow us to reach surface brightness limits much below 30 mag arcsec^{-2}. At distances greater than a few Mpc, only the integrated light is available with the current facilities. The limiting factors are then not only the exposure time but also, and as importantly, the sky background level, the flat-field subtraction, the scattered light from bright stars and the field of view. Most efforts in the detection of extremely low surface brightness structures around galaxies have so far been done for spirals; they have for instance led to the discovery of a stellar bridge linking the Local Group galaxies M31 and M33 (McConnachie et al. 2009), or spectacular streams around nearby spirals (Martínez-Delgado et al. 2010).

In the hierarchical scenario, ETGs should exhibit even more fine structures than late-type galaxies (see simulations by Johnston et al. 2008; Michel-Dansac et al. 2010b; Peirani et al. 2010). Unfortunately, in clusters of galaxies where ETGs prevail, the fine structures are particularly fragile and are easily destroyed. Multiple stellar streams were none the less recently disclosed by two dedicated deep surveys of the Virgo Cluster with the Burrell Schmidt telescope (Mihos et al. 2005; Janowiecki et al. 2010) and the Canada–France–Hawaii Telescope (CFHT) as part of the Next Generation Virgo Cluster Survey (NGVS; Ferrarese et al., in preparation). Tal et al. (2009) have, however, confirmed that streams are more frequent in field ETGs where they should be longer lived. van Dokkum (2005) collected on deep optical images of cosmological fields a large sample of red anonymous ETGs located at a median redshift of 0.1 and identified around them tidal debris. He claimed that 70 per cent of the bulge-dominated galaxies show tidal perturbations telling about a recent merger. In parallel, the frequent presence of gaseous streams around ETGs has been disclosed by H I surveys carried out with the Very Large Array (e.g. Schiminovich et al. 1995; Sansom, Hibbard & Schweizer 2000), with the Australia Telescope Compact Array (Oosterloo et al. 2007) or the Westerbork Synthesis Radio Telescope (WSRT) (Oosterloo et al. 2010).

Prompted by these theoretical studies and early observations and capitalizing on the wealth of ancillary data obtained by the ATLAS^{3D} project, we have initiated a deep imaging survey of very nearby, well-known, ETGs in isolation or in groups. The observations, carried out with the wide field-of-view MegaCam camera installed on the CFHT, allow us to study the morphology of the selected galaxies out to very large radius, obtain maps of their outskirts at unprecedented depth and study their even larger-scale environment.

We report in this paper results obtained on two ellipticals of the ATLAS^{3D} sample, NGC 680 and 5557, that belong to the two principal sub-classes of ETGs: slow and fast rotators. Both turn out to exhibit in their surrounding spectacular tidal features. The optical observations and data reduction, as well as the data gathering of ancillary data, including H I maps with the WSRT, are detailed in Section 2. The detection and characterization of their outer fine structures, including tidal dwarf galaxies (TDGs) candidates, are presented in Section 3 and a link is made to the inner properties of the two galaxies. Finally in Section 4, we discuss the merger scenario for the origin of these two specific systems, and address their representativeness among the ATLAS^{3D} galaxies.

2 OBSERVATIONS AND DATA REDUCTION

2.1 The two targets

The two selected targets presented in this paper, NGC 680 and 5557, lie at roughly the same distance: respectively 37.5 and 38.8 Mpc (Paper I).[1] Both are classified as very early-type galaxies: $T < -4$ in the Leda classification (Paturel et al. 2003), respectively E2 and E1 with the de Vaucouleurs classification. They are roundish structures, with ellipticities ϵ between 0.15 and 0.2. With M_K of respectively -24.1 and -24.8 (Skrutskie et al. 2006), they are massive systems. Having specific angular momenta λ_R of respectively 0.46 and 0.05, NGC 680 and 5557 unambiguously belong to the classes of respectively fast and slow rotators (Emsellem et al. 2011, hereafter Paper III). The two galaxies were initially selected as targets for MegaCam observations because of the intriguing presence of H I clouds in their vicinity that showed no optical counterparts on the available images at that time (from the Sloan Digital Sky Survey and Isaac Newton Telescope; see details in Paper I). The H I data were obtained with a dedicated survey with the WSRT made as part of the ATLAS^{3D} project (Serra et al., in preparation). One motivation of the proposed deep optical imaging was the investigation of the nature of these clouds which could either be primordial accreted clouds or tidal debris. A paper based on MegaCam observations using a similar technique as this paper and revealing an optical counterpart to the gigantic H I structure in the Leo ring has been published by Michel-Dansac et al. (2010a).

2.2 Deep imaging with MegaCam

2.2.1 Observations

Deep optical images of NGC 680 and 5557 were obtained between 2009 January and September with the MegaCam camera installed on the CFHT. 1 deg^2 field of view images were obtained with the g', r' and i' bands.

Each observation in a given filter consisted of six exposures sequenced in time within a 45 min time window in order to minimize sky background variations due to the inevitable varying observing environment. Indeed since the true sky varies in the optical by a few per cent in shape (gradients) and intensity on time-scales of the order of 1 h, exposures used to build a sky must fit within such time window, and the dithering pattern around the object must be optimized to integrate the science field at all time. Since the MegaCam field of view is much larger than the scale of the observed objects, an extremely large dithering pattern is applied (at least 7 arcmin distance from centre to centre of all six images): this allows 100 per cent of the integration time to be spent on the science field while integrating the background sky all the while.

Such large dithering patterns ensure that all known optical artefacts plaguing MegaCam, especially the largest stellar haloes (6 arcmin) caused by internal reflections in the camera optics, can be rejected by building a master sky based on only six exposures. Without such approach, a single frame (or stack made of only slightly dithered frames) exhibits a large radial structure due to the use of twilight flat-fields convolved with a photometric response map offering a flat photometric response across the camera (Magnier & Cuillandre 2004; Regnault et al. 2009). Such data limit the detection of faint features against the sky background to a surface brightness of only 27 mag arcsec^{-2} over scales of only a few arcmin.

[1] There is an uncertainty in the real distance of NGC 5557. The adopted value is the mean of the redshift-independent distance determinations in the NASA/IPAC Extragalactic Data base. The latest value determined by Cantiello et al. (2005) based on the measure of the Surface Brightness Fluctuations of the galaxy is 47.9 Mpc. If this distance is true, the sizes of the tidal features detected by MegaCam should be multiplied by a factor of 1.2.

Table 1. MegaCam observations.

Galaxy	Band	N	Integration (s)	IQ (arcsec)	Background (ADUs)
(1)	(2)	(3)	(4)	(5)	(6)
NGC 680	g	6	882	0.95	277
	r	12	2760	0.71	726
	i	6	714	0.58	589
NGC 5557	g	6	882	1.37	191
	r	6	1380	1.12	364
	i	6	714	0.95	621

Notes. (3) Number of individual exposures. (4) Total integration time. (5) Image quality: FWHM of the point spread function. (6) Background level.

The number of exposures, total integration time, average seeing and background level is listed in Table 1. Weather conditions were photometric for all data set.

2.2.2 *Data reduction and sensitivity*

The data were processed at CFHT with the Elixir Low Surface Brightness arm of the MegaCam pipeline at CFHT, Elixir-LSB (Cuillandre et al., in preparation). The input data for the Elixir-LSB come from Elixir, the main pipeline which offers a full detrending of the individual frames, the correction of the camera photometric response, as well as the astrometric and photometric calibration. The output product of Elixir-LSB are single frames and stacks where the sky background has been modelled and removed, opening the possibility for photometry on extremely large scales (arguably the size of the field of view) as well as the detection of extremely faint structures above the background. Coupled to the proper observing strategy (see above), Elixir-LSB achieves in all bands a sky flattening of 0.2 per cent, nearly 7 mag fainter than the sky background. In the g band, this defines a detection limit at the 29th magnitude per arcsec^2 level. While inspired from infrared nodding observing techniques, the fundamental difference with optical data such as the MegaCam images is that the sky background is very low and the image signal is dominated by astronomical sources. Special filtering and rejection techniques are used in Elixir-LSB in order to reject these objects and derive the radial shape of the sky background across the camera field of view induced by the flat-fielding based on twilight sky exposures convolved with a photometric map correction (Magnier & Cuillandre 2004).

The sky-corrected individual images are then finely calibrated for astrometry and photometry by the software SCAMP (Bertin 2006) and subsequently resampled, skipping the usual internal sky subtraction, by the software SWARP (Bertin et al. 2002) at a pixel scale of 0.561 arcsec per pixel (3 × 3 binning) in order to boost the signal-to-noise ratio on faint extended objects. The stacks used in the science analysis are finally produced by an Elixir-LSB routine optimized for low numbers of input frames.

The images of the two observed fields, scaled in mag arcsec^{-2}, are displayed in Fig. 1. At the depth of the images, many foreground, faint, stars show up. Given the large extent of the studied structures and their very low surface brightness, the subtraction of the contaminating light from these stars as well as from distant unresolved galaxies becomes a critical issue. These sources were subtracted with a ring-filter technique (Secker 1995). The low surface brightness haloes of the brightest stars, and in general of all luminous objects, including the galaxies, are prominent on the MegaCam images and much more difficult to subtract. They are among the strongest sources of confusion, especially when close to the target galaxies.

2.2.3 *Galaxy subtraction*

The detection of the inner fine structures required the subtraction of the galaxies. To do this, their light profiles were modelled in 2D with GALFIT (Peng et al. 2002). As a first step, the images were rebinned

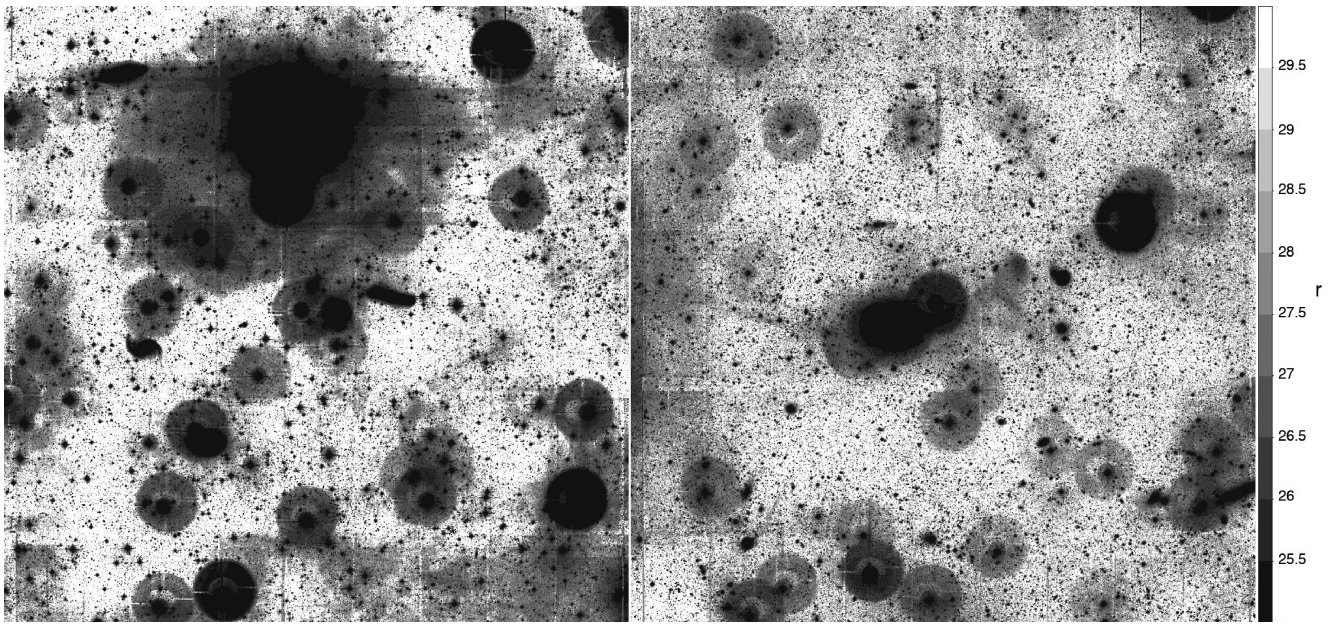

Figure 1. r-band surface brightness map of the 1 deg^2 MegaCam fields around NGC 680 (left) and 5557 (right). The two ETGs are located close to the centre of the images. The surface brightness scale is shown to the right. The images are displayed with cuts between 25 and 30 mag arcsec^{-2} to enhance the structures with the faintest surface brightness: instrument signatures, foreground stars, stellar haloes, galactic haloes and collisional debris. At the distance of NGC 680 and 5557, 1° corresponds to, respectively, 650 and 670 kpc. North is up and East is towards left.

and the stars and other bright objects – except the target – masked. The masks were created from the images from which the large-scale structures had been subtracted. The pixels defining the masks were selected based on their signal-to-noise ratio and a threshold value manually adjusted to ensure the detection of the faintest stars. The noise and sky levels were then estimated fitting the histogram of the intensity distribution of the residual images with a Gaussian.

Both NGC 680 and 5557 were fitted by a de Vaucouleurs profile, i.e. fixing a Sersic index to 4. Relaxing the value of this index, or adding additional components, did not decrease significantly the residuals. Note that our study mainly addresses collisional debris far out from the ellipticals; thus our results do not suffer much from uncertainties in the galaxy modelling.

2.3 Ancillary data from ATLAS^{3D} and *GALEX*

Most of the ancillary data used in this study were taken as part of the ATLAS^{3D} survey and their acquisition and data reduction described in dedicated papers. In particular, the H I data shown in this paper were extracted from a survey carried out with the WSRT. The full width at half-maximum (FWHM) of the WSRT primary beam was 36 arcmin. Each galaxy was observed for 12 h with 1024 frequency channels covering a bandwidth of 20 MHz. This corresponds to a channel width of $\sim$4 km s^{-1} over a velocity range of $\sim$4000 km s^{-1}. Data were reduced using a pipeline based on the MIRIAD package (Sault, Teuben & Wright 1995). The total-H I images shown in this paper are obtained from data cubes with an FWHM of 51 $\times$ 34 arcsec for NGC 680 and 39 $\times$ 36 arcsec for NGC 5557. The limiting column density is 2.2 and 2.8 $\times$ 10^{19} cm^{-2} for NGC 680 and 5557, respectively. More details on the H I observations are given in Serra et al. (in preparation).

Furthermore, deep UV data of NGC 5557 obtained in 2007 July were queried from the *GALEX* archives (PI program number 079028). The integration time in the NUV and FUV bands were about 1000 s.

3 RESULTS

3.1 Detection of new fine structures

The presence of some level of disturbances had already been reported in the two galaxies under study. Looking at CCD images, Ebneter, Davis & Djorgovski (1988) noted the possible presence of 'patchy dust' in NGC 680 while the structure of NGC 5557 is described as chaotic. Schweizer et al. (1990) derived a rather low but non-zero Σ index for the latter galaxy. As a matter of fact, hints for asymmetric structures in the outskirts of both ellipticals are barely visible on the shallow Isaac Newton Telescope (INT) and Sloan Digital Sky Survey (SDSS) images that were available before the CFHT observations presented here.

The ultra-deep MegaCam images revealed that the previously detected disturbances were real, and furthermore disclosed a wealth of so far unknown fine structures, such as shells and long tidal tails. They may be seen on the true colour (g, r, i) images shown in Figs 2 and 5 as well as on the single-band surface brightness maps shown in Figs 3 and 6. For future reference, the fine structures are labelled on the images shown in Figs 4 and 7 for which the galaxy models obtained with GALFIT have been subtracted.

3.1.1 NGC 680

Extended structures show up on each side of NGC 680. They are visible in the three observed bands. The halo of a bright star contaminates the emission of the southern stellar plume. Given the colour of the star, the effect is however strongest in the g and r bands. The r band has the longest exposure time (see Table 1) but suffers from a higher background level. For this specific system, the i-band image shown in Fig. 3 turned out to be the cleanest and most informative one. The two stellar plumes to the South-East and North-West of NGC 680 (TT-E and TT-W) are very broad, are diffuse and have medium projected lengths of, respectively, 75 and 60 kpc. Their surface brightness ranges between 26 and 28.5 mag arcsec^{-2} in the g band (25.5 and 28 mag arcsec^{-2} in the i band). The optical luminosity of the plumes contributes to about 2 per cent of the total optical luminosity of the galaxy.

NGC 680 belongs to a group of galaxies and has several close companions. The deep MegaCam images did not reveal any obvious stellar bridge between the elliptical and NGC 678 to the North-West. However, both galaxies have similar velocities (see Fig. 8) and are most likely already interacting. NGC 678 is an edge-on spiral showing a prominent dust lane along its disc, best visible in the $g - i$ colour map image displayed in Fig. 9. To the West, the dust lane seems to bifurcate. To the North-East, a warp is visible on the optical bands. All these features plus the thickness of the disc indicate that the spiral is likely disturbed. Its unfavourable orientation precludes the detection of tidal tails. The second companion, IC 1730, lies within a common very low surface brightness envelope, but for this galaxy as well, no clear bridge is distinguishable.

As shown in Fig. 2, the stellar plumes match well the extended H I structures mapped by the WSRT. The true colour image and $g - i$ colour map (Fig. 9) do not reveal any compact blue star-forming regions along the plumes, despite their gas richness. The existence of gaseous tails around NGC 680 was actually known from previous H I observations by van Moorsel (1988) who moreover disclosed numerous other intergalactic H I clouds further away from the galaxy.

The presence of apparently free floating clouds is confirmed by the WSRT data. The H I structures labelled as Clouds-S and Clouds-E do not show any optical counterpart at our sensitivity limit of 29 mag arcsec^{-2} while a dwarf galaxy is detected at the location of Cloud W (see insets in Fig. 2). The velocity map of Clouds-E and Clouds-S (Fig. 8) suggests that the H I structure is a tidal tail emanating from the interacting galaxies IC 167/ NGC 694 rather than from our target galaxy, NGC 680. Indeed there is a continuous velocity field from the galaxy pair to the tip of the H I structure.

At smaller galactocentric radius, the number of distinct stellar fine structures increases. One of the most prominent is a narrow arc to the East, which has a maximum surface brightness of 25.5 mag arcsec^{-2} in the g band (Arc-E on Fig. 4). This arc is much bluer than the surrounding material (see Fig. 9) and probably made of stars of different age or metallicity than the main body. Subtracting a model of the elliptical from the image, a few faint concentric shells show up (Shells 1, 2, 3 in Fig. 4). More towards the nucleus, brighter, asymmetric structures are disclosed. Whether they are real or an artefact of the model used here is unclear. In any case, the images and colour map of the central regions of NGC 680 suggest a rather high level of disturbances, which might be due to some remaining star formation activity (see discussion in Section 3.4.2 on that matter).

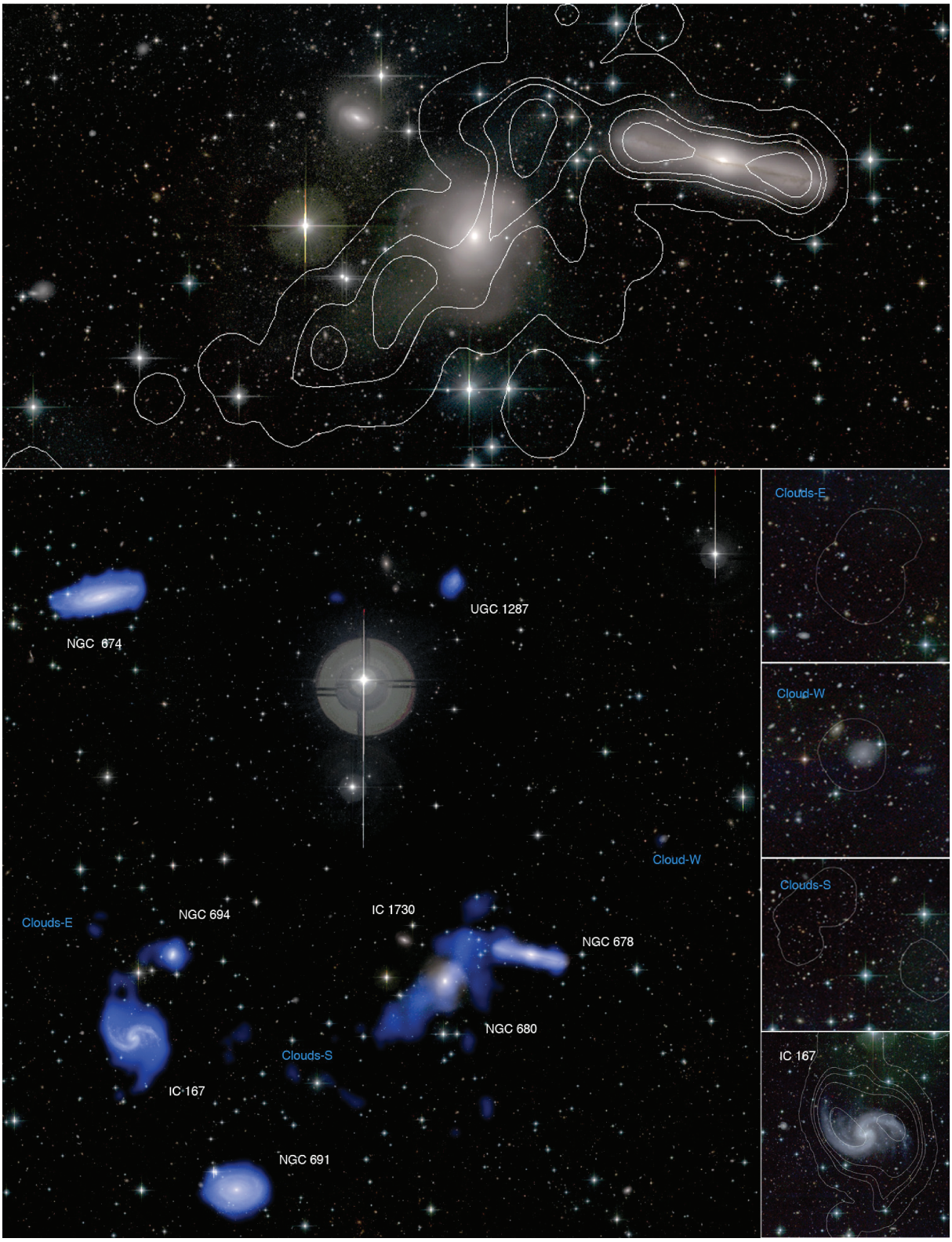

Figure 2. Bottom left: CFHT/MegaCam true-colour (composite of the *g, r, i* bands) image of the NGC 680 group of galaxies. The distribution of the H I gas mapped by the WSRT is overlaid in blue. North is up and East towards left. The field of view is 49.0 × 47.0 arcmin^2 (535 × 513 kpc, at the distance of the galaxy). Top: close up towards NGC 680 and its closest companions. The contours of the H I emission (levels: $N_{\rm H\,I}$ = 2, 12, 20, 36 × 10^{19} cm^{-2}) are superimposed on the true colour image. Bottom right: close up towards the intergalactic H I clouds in the group and the interacting galaxy IC 167.

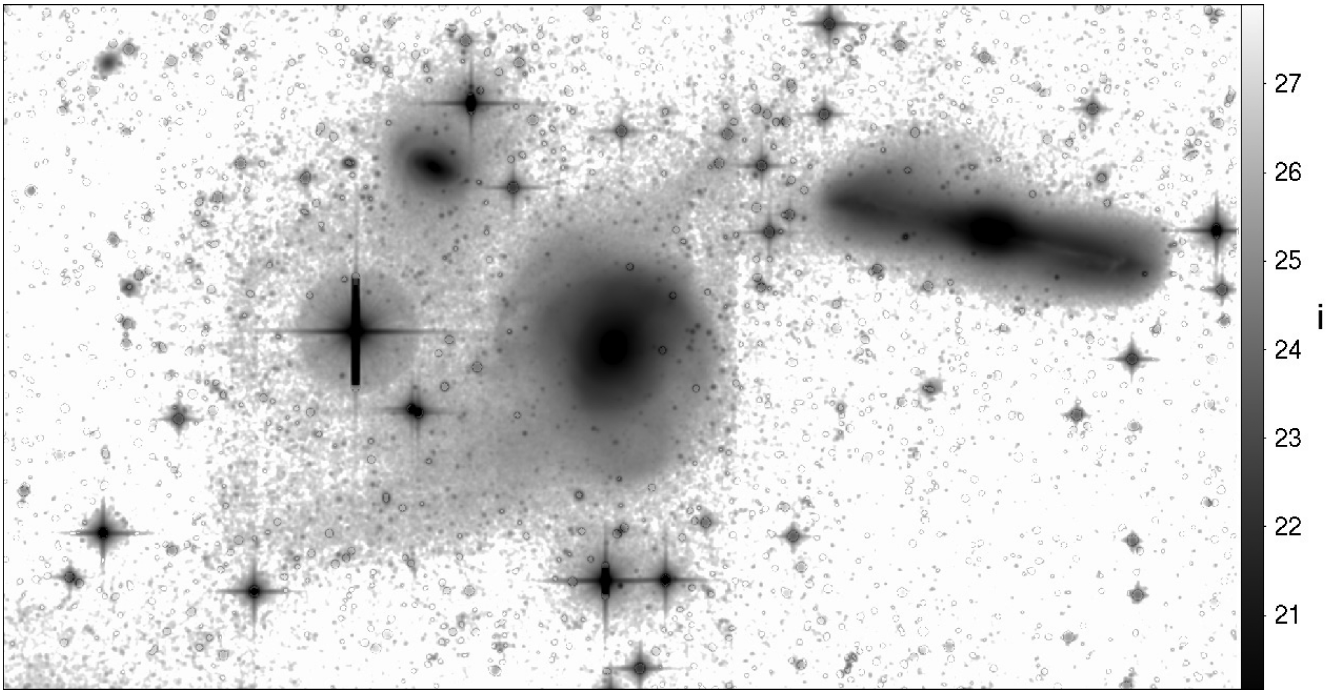

Figure 3. CFHT/MegaCam *i*-band surface brightness map of NGC 680. The surface brightness scale in mag arcsec^{-2} is shown to the right. The faint foreground stars and distant background galaxies were subtracted from this map. North is up and East towards left. The field of view is 17 × 10 arcmin^2 (212 × 125 kpc, at the distance of the galaxy).

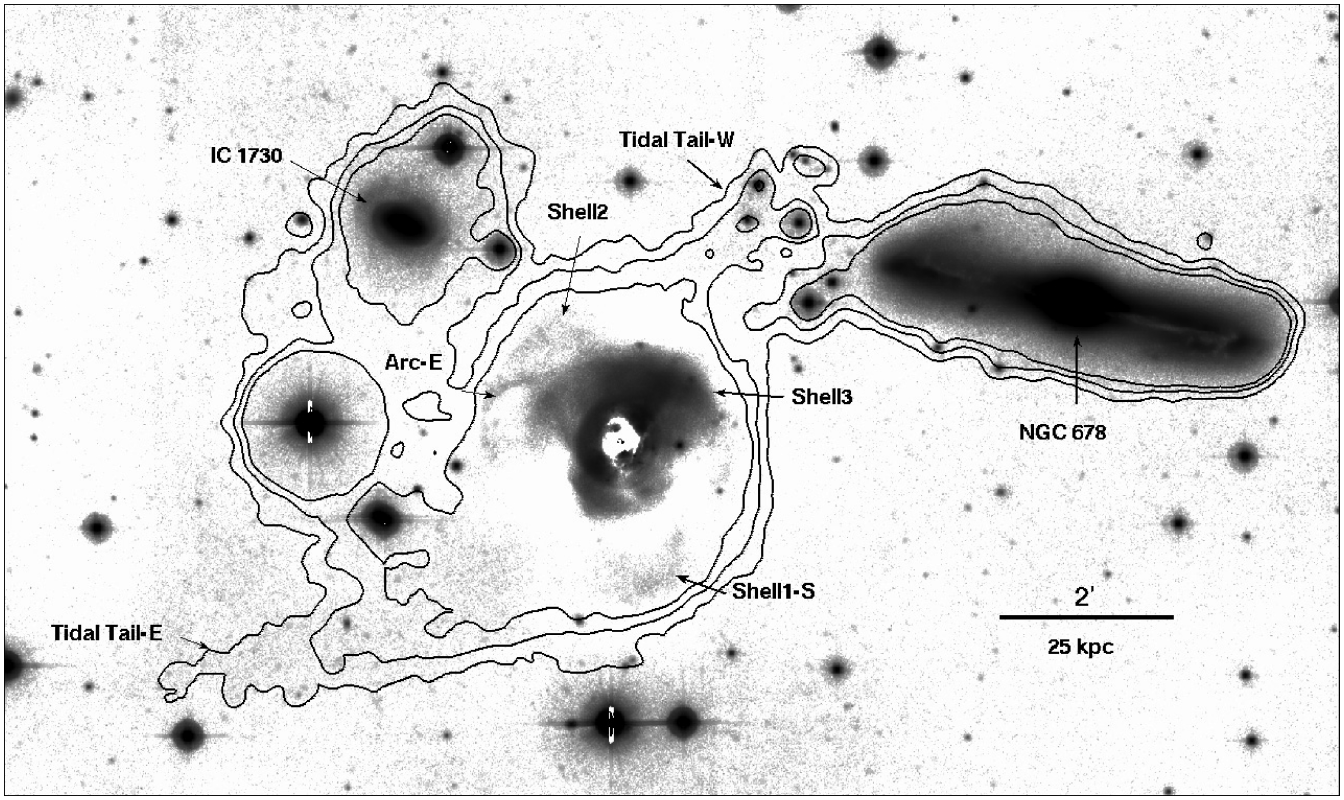

Figure 4. *g*-band surface brightness map of NGC 680, after the subtraction of a galaxy model with a single Sersic index of 4. The faint foreground stars and distant background galaxies have been subtracted from the image. The contours of the galactic emission before the galaxy subtraction, as shown in Fig. 3, are superimposed (levels: 28, 27 and 26 mag arcsec^{-2}). The various fine structures disclosed by the image are labelled.

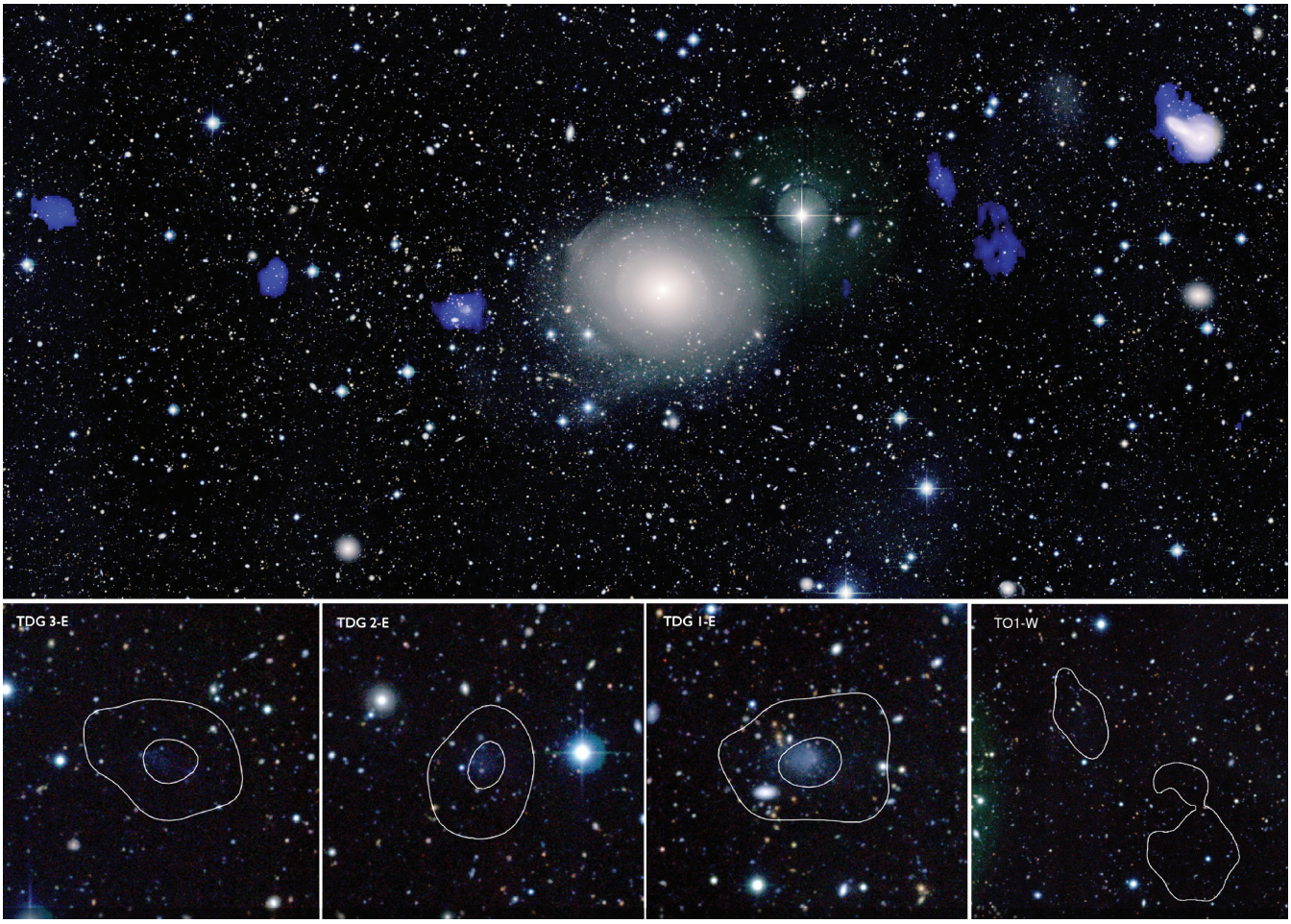

Figure 5. Top: CFHT/MegaCam true-colour (composite of the *g, r, i* bands) of NGC 5557. The distribution of the H I gas mapped by the WSRT is overlaid in blue. North is up and East towards left. The field of view is 39.5 × 18.8 arcmin^2 (446 × 212 kpc, at the distance of the galaxy). Bottom: close-up towards the intergalactic H I clouds around the galaxy. Fields of view are 3 × 3 arcmin^2 for TDG1–3-E and 5 × 5 arcmin^2 for TO1-W. The H I contours from the robust weighted map (levels: $N_{H2} = 3, 12 \times 10^{19}$ cm^{-2}) are superimposed on the true colour images (*g, r, i*). The H I clouds to the East exhibit blue optical and UV (*GALEX*) counterparts and are TDGs candidates. The clouds to the West have extremely faint counterparts (see Fig. 6).

3.1.2 NGC 5557

The most striking optical structures of NGC 5557 are, to the East, a long straight, narrow, filament (Tidal Tail-E in Fig. 7), and to the West a broader, more complex structure, apparently composed of an extended object at its tip (TO2-W), a ring (R-W) and a bridge (TO1-W). We will argue in the following that some of these features are the optical counterparts of the apparent free-floating H I gas clouds that had previously been detected around the ETG by the WSRT.

The Eastern tail stretches out from the diffuse halo around the elliptical; it is lost 15 arcmin further to the East in a region of the MegaCam frame with a high local background that could not be removed (see Fig. 1). Its projected distance is at least 160 kpc. The filament is clearly visible in the *g* (Fig. 6) and *r* (Fig. 1) bands; its average surface brightness is, however, very low: 28.5 mag arcsec^{-2} in the *g* band. At three positions along the tail, the surface brightness increases to 25–26 mag arcsec^{-2}; these clumps (TDG1-E, TDG2-E, TDG-3-E) appear to be rather blue on the true colour image shown in Fig. 5, and most likely correspond to star-forming regions, as further suggested by their detection in the *GALEX* far-ultraviolet band. Each of them is associated with an individual H I cloud (see Fig. 5). As argued in Section 3.3, these blue, star-forming, gas-rich, objects host by a redder filament are likely TDGs, which condensed out of material expelled during the galaxy–galaxy collision.

The western structure is much more difficult to interpret. Its base towards NGC 5557 is lost within the halo of a bright red star. In the *g*-band image shown in Fig. 7, there seems to be an extension south of the star, linking the galaxy to object TO1-W. Between the 26 mag arcsec^{-2} isophote of the elliptical and its western most tip, the structure has a projected size of 11.9 arcmin, or 130 kpc at the adopted distance of NGC 5557. Its surface brightness is at its maximum towards TO2-W where it reaches 26 mag arcsec^{-2}. As shown in the $g - i$ colour map (Fig. 10), TO2-W has the same colour as the outer region of the elliptical. Besides the presence of a bridge, the similar colour suggests that the western structure and the outer regions of the galaxy are composed of similar stellar material, implying that TO2-W is made of tidal debris as well. Other interpretations are however possible, as discussed in Section 4.1. The ring-like structure R-W is in particular intriguing. West of NGC 5557, TO1-W and possibly R-W are the only objects detected in H I.

Overall, the distance between the two extreme tips of the low surface brightness structures on each side of NGC 5557 (i.e. between TDG3-E and TO2-W) is 375 kpc, making it, if indeed physically

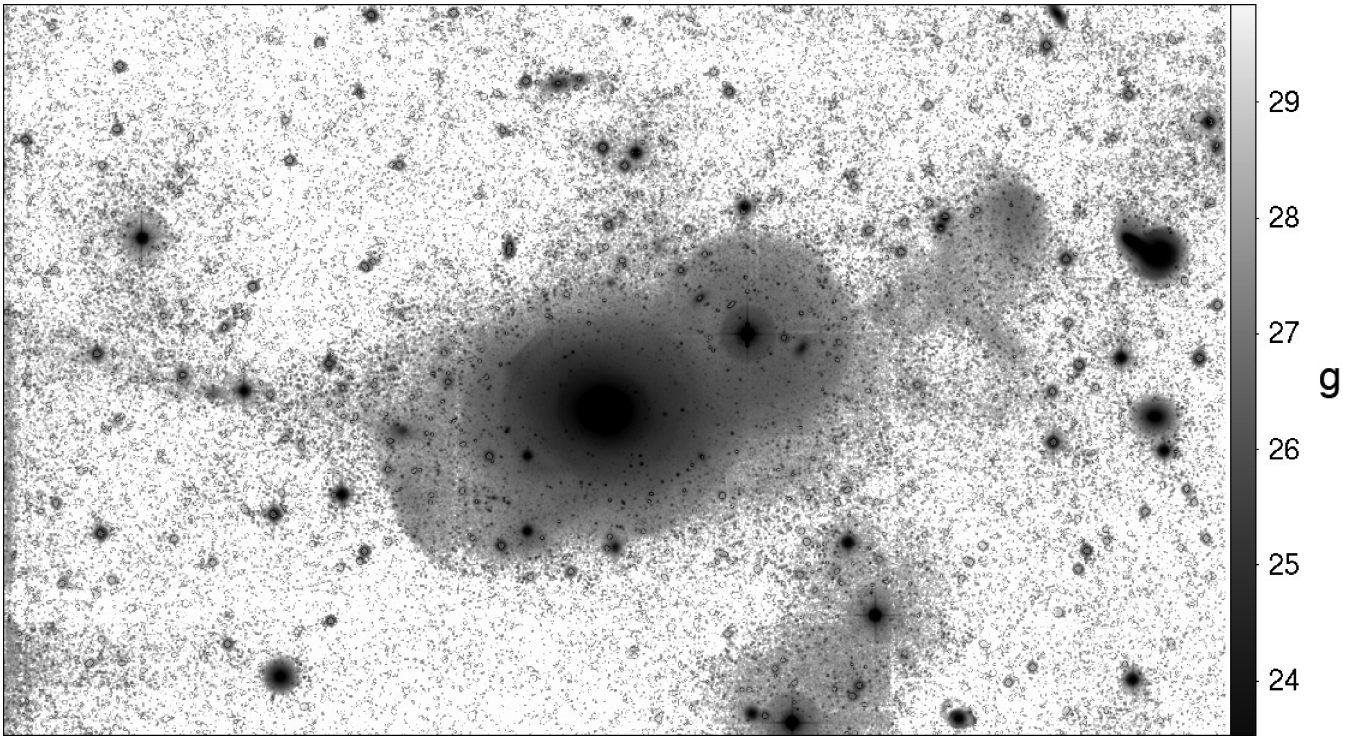

Figure 6. CFHT/MegaCam *g*-band surface brightness map of NGC 5557. The surface brightness scale in mag arcsec^{-2} is shown to the right. It ranges between 23 and 30 mag arcsec^{-2}. The faint foreground stars have been subtracted. North is up and East towards left. The field of view is 37.0 × 22.7 arcmin^2(418 × 256 kpc, at the distance of the galaxy).

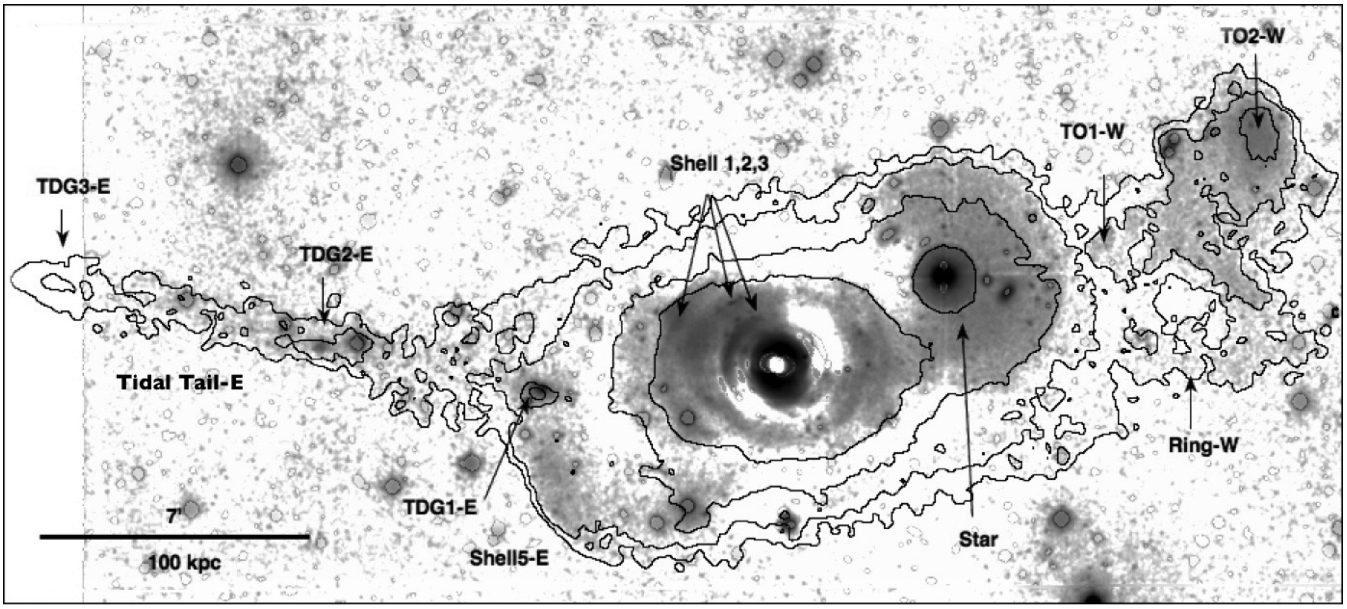

Figure 7. *g*-band surface brightness map of NGC 5557, after the subtraction of a galaxy model with a single Sersic index of 4. The faint foreground stars have been subtracted from the image. The contours of the galactic emission before the galaxy subtraction, as shown in Fig. 6, are superimposed (levels: 29, 28, 27 and 26 mag arcsec^{-2}). The various fine structures disclosed by the image are labelled. The image is cut to the East at a location where a high sky background could not be properly removed (see Fig. 1).

connected, one of the largest stellar structures ever observed around a galaxy. As comparison, the tidal tails of the well-known prototypical merger, the Antennae, have a maximum size of 100 kpc, while the so-called Superantennae, a more distant merging system which is ultraluminous in the far-infrared, have a total extent of 350 kpc (Mirabel, Lutz & Maza 1991).

Getting closer to the central regions of the elliptical, several additional features are visible, starting with a shell (Shell5-E), located

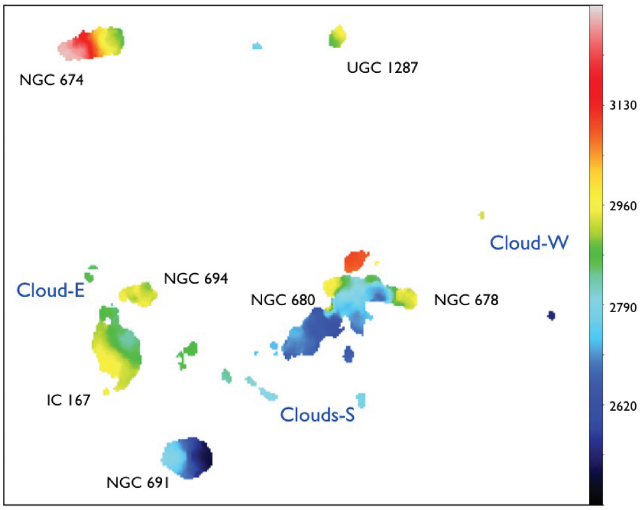

Figure 8. The velocity map of the H I emission in the NGC 680 group of galaxies. The intensity scale in km s^{-1} is shown to the right. The field of view is 0.°8 × 0.°7.

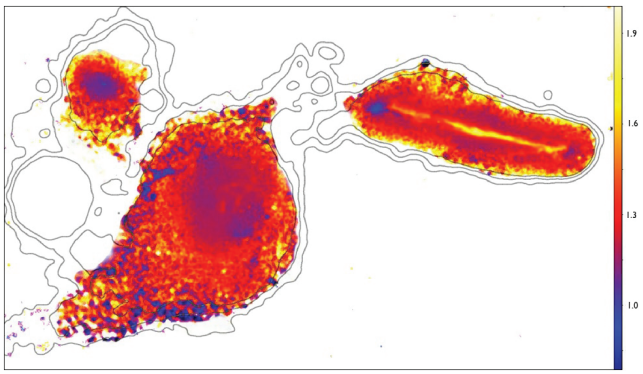

Figure 9. $g - i$ colour map of NGC 680. All foreground stars have been subtracted. The contours of the surface brightness maps with the same levels as in Fig. 4 are superimposed.

at 80 kpc from the nucleus. There the surface brightness suddenly drops below the detection limit of 29 mag arcsec^{-2}. Furthermore, the images shown in Figs 5 and 6 reveal two shells (S1 and S2) with g-band surface brightness of about 25.5 mag arcsec^{-2}. These are probably part of a series of concentric ripples. The inner most ones are disclosed subtracting a model of the elliptical from the image (see Fig. 7). Artefacts of the method for the galaxy modelling with GALFIT become prominent in the innermost regions. However, shell S3 is also present when subtracting a galaxy modelled by an ellipse fitting algorithm ('ellipse' within IRAF) and is probably real.

These shells do not show up on the $g - i$ colour map shown in Fig. 10. There is thus no hint that their stellar population differs from the one of the parent galaxy and comes from an external accreted galaxy containing stars with radically different age or metallicity, like for a disrupted dwarf satellite. The bluer shell around NGC 680 is in that respect much different. Despite the presence of faint shells, the central regions of NGC 5557 have overall very regular isophotes, as expected for a fully relaxed galaxy. The study of the most external regions reveal a much more disturbed history.

3.2 Characterization of the fine structures

To summarize, our MegaCam images have allowed us to considerably increase the number of detected fine structures both in NGC 680 and in NGC 5557. To quantify this, we used the empirical approach of Schweizer et al. (1990), and computed the fine structure index Σ, defined as $\Sigma = S + \log(1 + n) + J + B + X$, where S is the strength of the most prominent ripples, n the number of observed ripples, J the number of jets, i.e. tidal structures, B and X, two indexes characterizing the inner morphology (Boxiness and 'X-structure'). Schweizer et al. (1990) had already determined it for NGC 5557, based on the shallow CCD images available at that time. The value of $S + B + X$ has in principle not changed with the new imaging; n has doubled with the detection of the outer shells, and the number of tidal structures went from 0 to at least 3 (TT-E,TO1/2-W,R-W). Therefore, the value of Σ should increase from 2.78, the value determined by Schweizer et al. (1990), to 6. NGC 680 was not in the sample of Schweizer et al. (1990). None the less, we have tried to roughly determine its fine structure index, estimating S to the intermediate value of 2, giving to n a minimum of three 'ripples', to S 3 tails and arc, 0 to B (no indication of a boxinesss) and 1 to X (tentative X structure). With all these assumptions, Σ amounts to 6.6. The updated values of the fine structure index bring both galaxies close to that of the prototypical advanced mergers NGC 3921 (8.8) and NGC 7252 (10.1) (Schweizer & Seitzer 1992).[2]

Alternatively, the level of tidal perturbations may be determined using less-subjective parameters such as the so-called 'Tidal parameter', T, defined by Tal et al. (2009) as the residual of the galaxy model subtraction. T quantifies all deviations from regular models obtained, for instance, by fitting the galaxy with elliptic light profiles. However, such a parameter turned out not to be functional for our study as it is not able to disentangle between major and minor mergers. Indeed, the newly discovered very extended tidal tails – which are clear signposts of a past prominent mass assembly event – have little impact on the measure of the tidal index, because of their very faint luminosity.

3.3 Intergalactic H I clouds and tidal dwarf galaxies

The WSRT survey has disclosed several apparently isolated intergalactic H I clouds around both NGC 680 and 5557. The least massive of them, East and South of NGC 680 (see Fig. 2), with column densities below 10^{20} cm^{-2}, are apparently collisional debris from the on-going interactions in the group, but do not exhibit optical counterparts at our sensitivity. A blue optical object is found towards Cloud-W. Its relative isolation in the NGC 680 group and velocity suggest that it is a pre-existing H I-rich dwarf galaxy.

On the other hand, the three blue objects aligned along the redder Eastern tidal tail of NGC 5557 appear as TDG candidates. A discussion on their real nature is given in Section 4.2. Their global properties are presented in Table 2 and their images shown in Fig. 5. The closest to NGC 5557, TDG1-E lies at the border of the extended stellar halo of the massive elliptical and the base of its tail. The most distant one, at more than 200 kpc from the galactic nucleus, is located near the tip of the tail. The central surface brightness of all

[2] Note that the tidal index is unlikely to change significantly, should the depth of the observations further increase, as confirmed by numerical simulations of binary mergers (Michel-Dansac et al. 2010b).A single major merger produces a limited number of tidal tails, generally four, two for each progenitor. Our deep observations basically allowed us to reveal structures that became fainter with time.

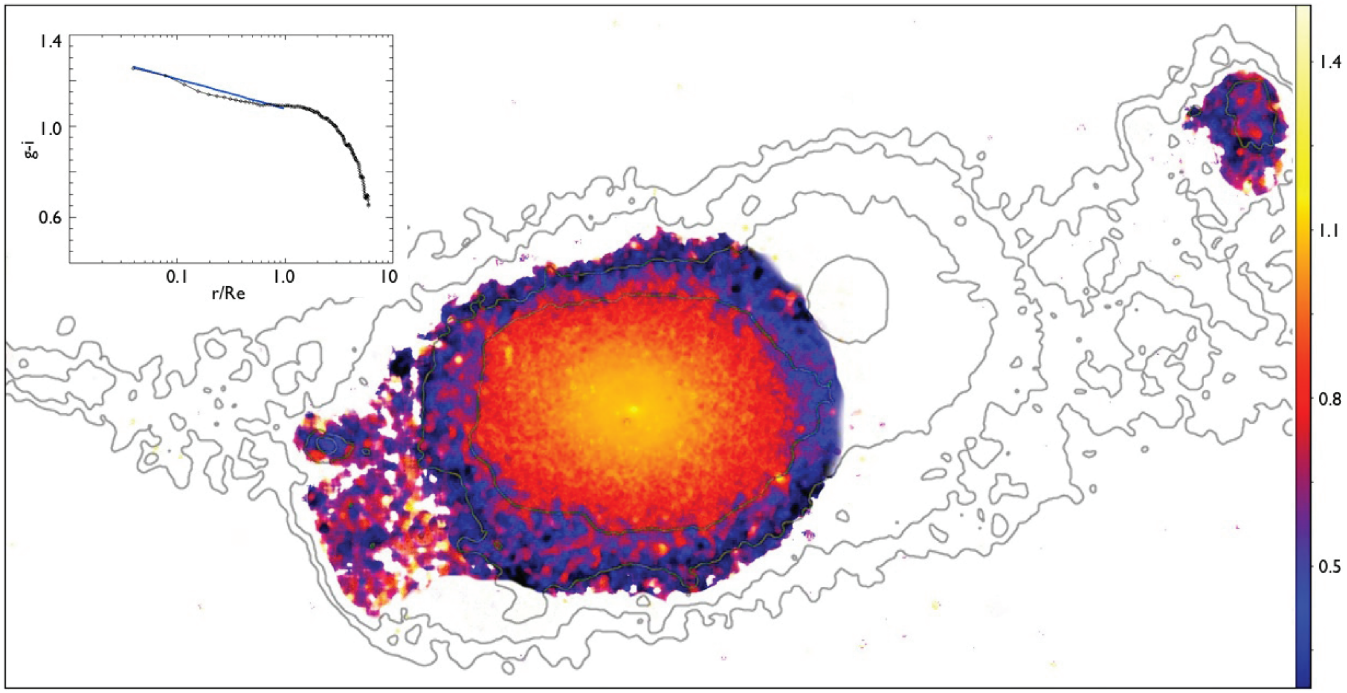

Figure 10. $g - i$ colour map of NGC 5557. All foreground stars have been subtracted. The contours of the surface brightness maps with the same levels as in Fig. 4 are superimposed. The inset shows the average colour profile as a function of radius. The blue curve corresponds to the mean colour gradient of a large sample of SDSS ETGs with average $g - i$ colours and Re similar as NGC 5557 (Tortora et al. 2010).

Table 2. Integrated properties of the TDG candidates in NGC 5557.

Name	RA	Dec.	d (kpc)	V (km s^{-1})	μ_{B0} (mag arcsec^{-2})	M_B (mag)	M_{HI} (10^8 M$_\odot$)	M_{HI}/L_B (M$_\odot$/L$_\odot$)	SFR(UV) (10^{-3} M$_\odot$ yr^{-1})
(1)	(2)	(3)	(4)	(5)	(6)	(7)	(8)	(9)	(10)
TDG1-E	14:18:55.9	+36:28:57	69.7	$3252 \pm 1 \pm 5$	25.3 ± 0.2	-14.05 ± 0.05	1.4 ± 0.2	2.2 ± 0.4	5 ± 0.5
TDG2-E	14:19:24.4	+36:30:05	134.3	$3196 \pm 1 \pm 2$	26.4 ± 0.3	-12.6 ± 0.1	0.8 ± 0.1	5.2 ± 1.1	2 ± 0.5
TDG3-E	14:19:58.1	+36:31:53	212.1	$3165 \pm 2 \pm 5$	26.9 ± 0.3	-12.6 ± 0.1	1.2 ± 0.2	6.7 ± 1.7	4 ± 1

Notes. (4) Projected distance to the nucleus of the parent galaxy. (5) Heliocentric velocity, determined fitting the peak of the H I spectrum integrated over the area of the TDG. The first value of the error is estimated from the Gaussian fit. The second value of the error takes into account the velocity gradient observed along the TDG. (6) Central surface brightness in the *B* band. (7) Absolute blue magnitude in the *B* band. *B*-band values were extrapolated from measurement in the *g* and *r* bands using the SDSS calibration by Lupton (2005). (8) H I mass. The errors given are estimated from the integrated spectra obtained with natural and robust weighted WSRT datacubes. (9) H I mass to blue luminosity. (10) SFR estimated from the *GALEX* FUV luminosity.

three objects exceeds 25.3 mag arcsec^{-2} ; they were therefore barely visible on previous maps of the region.

Their blue optical colour and detection in the far-UV (see Table 3) tell that the dwarfs exhibit an on-going star formation activity. The star formation rate (SFR), as estimated from the *GALEX* UV fluxes with the formula SFR(UV) $= 1.4 \times 10^{-21}$ L$_\nu$ [W Hz^{-1}] M$_\odot$ yr^{-1}(Kennicutt 1998), is modest: 0.005 M$_\odot$ yr^{-1} for the most active galaxy. In agreement with the presence of young stars, the three dwarfs were detected in H I, with a rather high M_{HI}/L_B ratio of 2–7 M$_\odot$/L$_\odot$.

3.4 Hints from the multi-wavelength data on the central regions

Our deep MegaCam optical images of the two target galaxies tell about a rich past accretion/merging history. Could it have been inferred analyzing the complementary multi-wavelength data of the ATLAS^{3D} survey, available for their central regions? In this section we present results based on the survey data taken with the SAURON integral field spectrograph (Paper I), which provides key information on the stellar populations, age and kinematics. We also use survey observations of the atomic gas obtained at WSRT (Serra et al., in preparation) and of the molecular gas taken with the IRAM 30-m telescope (Paper IV).

Table 3. Photometry of the TDG candidates in NGC 5557.

Name	FUV	NUV	g (mag)	r	i
TDG1-E	20.7 ± 0.1	19.8 ± 0.1	18.5 ± 0.05	18.0 ± 0.05	17.7 ± 0.05
TDG2-E	21.6 ± 0.2	20.6 ± 0.2	20.1 ± 0.05	19.8 ± 0.05	19.3 ± 0.05
TDG3-E	20.9 ± 0.2	20.1 ± 0.2	20.1 ± 0.1	19.9 ± 0.1	19.8 ± 0.1

3.4.1 Stellar kinematics

The dynamical and kinemetric analysis based on the ATLAS^{3D} SAURON data are summarized here:

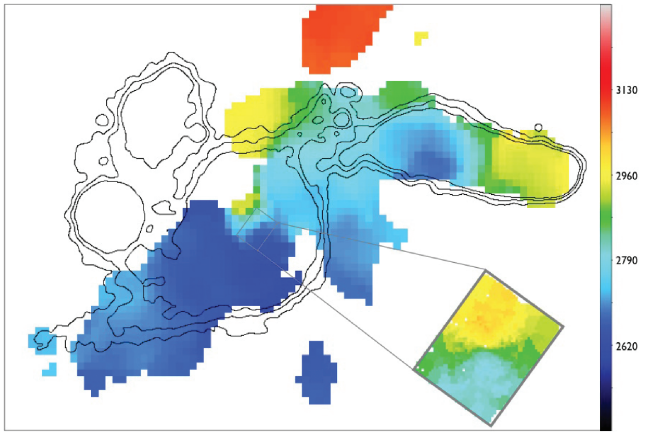

Figure 11. Velocity map of NGC 680. The main figure shows the H I velocity map from WSRT while the inset presents the stellar velocity map from SAURON. The contours of the surface brightness maps with the same levels as in Fig. 4 are superimposed. The velocity scale in km s^{-1} is shown to the right.

(i) The stellar velocity map of NGC 680, shown in the inset of Fig. 11, undoubtedly suggests regular rotation. The galaxy belongs to the ATLAS^{3D} group 'e' of *Disc Rotators* (Paper II). With a specific angular momentum λ_R of 0.46 within half of the effective radius, it is a clear fast rotator (Paper III). There is a misalignment angle of about 37° between the kinematic position angle (359°.5) of the stellar component in the inner regions (Paper II) and that inferred further out from the H I data. Finally, despite its rather perturbed central morphology (see the previous section), the galaxy does not show any remarkable kinematic feature within the SAURON field of view (33 × 41 arcsec^2; 6 × 7.4 kpc), such as a decoupled core. This is, however, typical of the fast rotators in the ATLAS^{3D} sample.

(ii) In sharp contrast, the stellar velocity map of NGC 5557, presented in the inset of Fig. 12, only exhibits weak evidence of rotation. The galaxy belongs to the ATLAS^{3D} group 'b' of *Non-Disc like Rotators*, with a maximum $V_{\rm rot}$ of 20.5 km s^{-1}. With a specific angular momentum at one half effective radius of $\lambda_R = 0.044$ while its apparent ellipticity is $\epsilon = 0.144$, the galaxy matches the criteria to be classified as a slow rotator (Paper III). No specific kinematical structure is observed.

3.4.2 *Stellar populations*

The SAURON data allow us to determine the principal characteristics, in particular the age, metallicity and abundance ratio, of the stellar populations in the central regions of the target ETGs. The method which makes use of the line strength index maps of Hβ, Fe5015 and Mgb and predictions from single stellar population models is described in Kuntschner et al. (2010) and McDermid et al. (in preparation). Outside the field of view of SAURON, the stellar populations may be constrained using their broad-band colour profiles.

(i) The SSP-equivalent mean value of the stellar age of NGC 680 within the central 0.3 kpc (Re/8) is 7.8 Gyr. It decreases to 6.5 Gyr within the effective radius (14 arcsec or 2.6 kpc) (McDermid et al., in preparation). The detection by SAURON of ionized gas (as traced by the [O III]$_{\lambda 5007}$ and Hβ emission lines) towards the nuclear region might indicate the presence of hot young stars. However, as recently pointed out by Sarzi et al. (2010), in ETGs most of the ionizing photons are emitted by old stellar populations, in particular the post-asymptotic giant branch (pAGB) stars. The near and far ultraviolet emission detected by *GALEX* of the core of the galaxy might as well reveal the presence of young stars, but it is now established that one of the main contributors of the UV emission of ETGs are old helium-burning stars (O'Connell 1999). Contamination by the UV-upturn (e.g. Gil de Paz et al. 2007, and references therein) makes it difficult to determine the SFR of ETGs from their UV emission. Up to 4 Re, NGC 680 has a rather uniform red $g - i$ colour, with a mild blueing by up to 0.15 mag towards the inner regions (see Fig. 9).

(ii) The SSP-equivalent mean value of the stellar age of NGC 5557 within the central 0.7 kpc (Re/8) is 8.1 Gyr. It decreases to 7.4 Gyr within one effective radius (29 arcsec or 5.4 kpc) (McDermid et al., in preparation). For comparison, at Re/8, Denicoló et al. (2005) estimated an age of 7 ± 1.3 Gyr, consistent with our determined value. There is no evidence of the presence of ionized

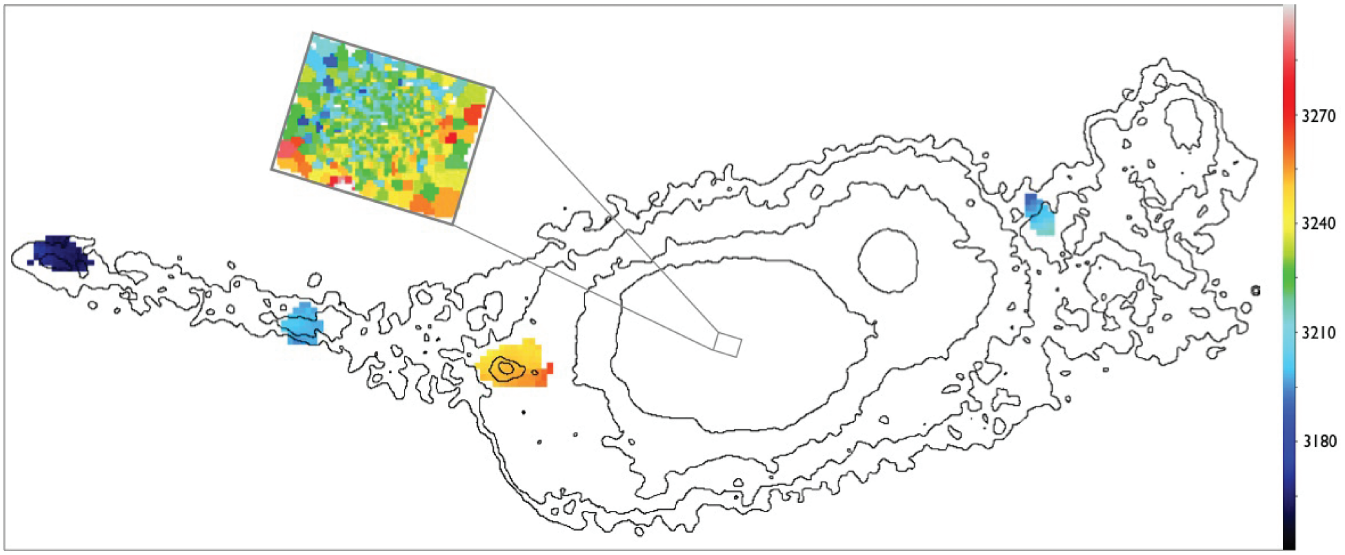

Figure 12. Velocity map of NGC 5557. The main figure shows the H I velocity map from WSRT while the inset presents the stellar velocity map from SAURON. The contours of the surface brightness maps with the same levels as in Fig. 4 are superimposed. The velocity scale in km s^{-1} is shown to the right.

hydrogen towards the nucleus of NG 5557: the $[O\,III]_{\lambda 5007}$ and Hβ emission lines were not detected by SAURON. As shown in Fig. 10, NGC 5557 exhibits a positive $g - i$ colour gradient (i.e. centre being redder). Up to 1 Re, the gradient is similar to that measured by Tortora et al. (2010) for a sample of nearby ETGs selected in the SDSS showing the same effective radius and mean colour as NGC 5557 ($g - i = 1.2$). As argued by Tortora et al. (2010), the colour gradient is likely due to a positive metallicity gradient. Beyond 2 Re and up to 6 Re, the gradient steepens. The average apparent drop by about 0.4 mag is only partly due to the contamination by the halo of the bright star to the West. According to single stellar population models (Bruzual & Charlot 2003), if only driven by metallicity, such a gradient would require a drop of metallicity by a factor of at least 100 of the old stellar component. The bluer colour in the very outskirts of the galaxy might reveal the presence of a population of stars with ages younger than 2 Gyr. Going even further out in the Western halo and collisional debris, the average colour increases, except towards the H I-rich star-forming objects located in the tidal tail.

3.4.3 Gas content

The CO(1–0) and CO(2–1) emission lines of the two galaxies were observed with the IRAM 30-m antenna as part of the ATLAS^{3D} survey (Young et al. 2011, Paper IV). They were not detected: the upper limits for the molecular gas mass are $\log(M_{H_2}) < 7.87$ M$_\odot$ and $\log(M_{H_2}) < 7.92$ M$_\odot$ for, respectively, NGC 680 and 5557, assuming a linewidth of the CO lines of 300 km s^{-1}. The absence of molecular gas in NGC 5557 is consistent with its low dust content – the galaxy was not detected at 160 μm by *Spitzer* (Temi, Brighenti & Mathews 2007) – and the lack of atomic and ionized hydrogen in the central regions. The only H I detected in this system by our WSRT observations is towards the four star-forming objects along the stellar Eastern and Western filaments. Earlier on, van Driel et al. (2001) had obtained an upper limit of $\log(M_{HI}) < 9.17$ M$_\odot$ using the Nançay antenna.

The absence of detected H_2 in NGC 680 may appear more puzzling as the galaxy does contain some amount of atomic hydrogen though it is mostly concentrated towards the tidal debris (see Fig. 2). Within the central beam of IRAM, the H I column density does not exceed 2×10^{20} cm^{-2}. 8×10^8M$_\odot$ of H I was detected there, giving an upper limit for the mass ratio of M_{H_2} over M_{HI} of 1. The central regions of ETGs usually exhibit much higher M_{H_2} over M_{HI} ratios, up to 10 (Oosterloo et al. 2010).

We discuss in the following section whether the properties of the central regions in both galaxies – absence of KDCs and molecular gas, dominant old stellar populations – are consistent with the hypothesis of a rather recent mass assembly event, suggested from the study of the external regions and the detection there of prominent tidal tails.

4 DISCUSSION

4.1 A merger origin for NGC 680 and 5557

As summarized in Section 1, the origin of the ETGs has been debated for a long time. If high-redshift observations of massive elliptical-like galaxies (Cimatti et al. 2004) seem to be surprisingly well described by a monolithic collapse or a very intense episode of star formation; it is largely agreed that mergers should have played a key role in their mass assembly. The issue is in fact to determine when and how the mass assembly principally occurred: through old or recent binary major mergers, multiple minor mergers or a combination of them. As a clock for age-dating merger events, the fine structures might bring precious insights into these questions.

The high fine structure index measured in NGC 680 and 5557, close to that of prototypical mergers such as NGC 7252, would suggest a relatively recent major merger for both galaxies. We examine this hypothesis in the following sections.

4.1.1 Tidal debris versus camera artefacts and foreground objects

When discussing structures with brightness as low as 28 mag arcsec^{-2}, the question about their reality naturally arises. Residuals of CCD gaps in the camera, of background variations, reflections and ghosts of bright objects, plus the star haloes have indeed similar brightness. However, they usually generate geometric shapes, like grids, discs or very extended diffuse patterns, that differ significantly from that of the fine structures discussed here: narrow tails, shells and arcs, which are typical of collisional debris. Besides, these structures are detected in several bands, which comforts the hypothesis that they are not instrumental artefacts.

A more serious issue is the contamination by foreground cirrus. Extended scattered emission from Galactic interstellar clouds and red emission associated with photoluminescence (Witt et al. 2008) can mimic stellar streams, as recently pointed out by Cortese et al. (2010). Carrying out a multi-wavelength analysis of the colliding galaxies NGC 4435/38 in Virgo, these authors argued that what had previously been taken as a tidal tail in the system was most likely a Galactic cirrus. The cirrus hypothesis is particularly worth investigating for the objects referred as TO2-W and R-W in Fig. 7, given their rather puzzling shape. However, the IRIS 60/100 μm maps, queried from the archives of the *IRAS* satellite, do not show at these locations the presence of the extended far-infrared emission expected for a cirrus. The closest FIR source, 4 arcmin away, is associated with the colliding galaxies NGC 5544/45. In the far-UV which is also a reliable tracer of Galactic cirrus (Cortese et al. 2010), there is as well no hint for extended UV emission on the 1066 s exposure FUV image that was queried from the *GALEX* archives. In fact, both NGC 680 and 5557 are fortunately located in holes within Galactic interstellar clouds. TO2-W and R-W in NGC 5557 are then likely genuine collisional debris and might correspond to a tidal tail for the former and an arc, perhaps made of stars falling back on to their progenitors for the latter, or tidal structures observed with specific projection angles.

4.1.2 Minor versus major merger: where does the tidal material come from?

The tidal structures disclosed by the MegaCam images might either originate from a parent massive galaxy involved in a major merger or from low-mass disrupted companions. The huge size of the tidal tails (75 kpc and at least 160 kpc for, respectively, the filaments of NGC 680 and 5557) argues for the major merger scenario, i.e. a merger involving progenitors with mass ratios smaller than 1:4. Tidal forces can stretch the stars of disrupted low-mass satellites along large distances – e.g. up to 80 kpc for the stream associated with the Sagittarius dwarf galaxy which is being accreted by the Milky Way (Martínez-Delgado et al. 2004) – but the tails formed that way usually wrap around the host galaxy, and do not have the linear structure observed for TT-E in NGC 5557. The rare so-called threshing systems, i.e. tidally disrupted in-falling satellites on

radial orbits (Forbes et al. 2003; Sasaki et al. 2007), might form long straight tidal tails. Those are, however, characterized by a remaining red, compact, central core with two tails (a major one and a counter one) emanating from it at different angles. In the case of TT-E, only one single structure is observed hosting three perfectly aligned blue, diffuse condensations. As shown by Bournaud & Duc (2006), such TDGs are unlikely to form in mergers between galaxies with mass ratios above 1:4. The broader fuzzy tails on each side of NGC 680 are as well inconsistent with being the remnants of accreted dwarf satellites.

The Eastern filament of NGC 5557 resembles the long, star-forming, tidal tails observed in real and simulated prograde encounters like in the Antennae (Karl et al. 2010), Super-Antennae (Mirabel et al. 1991) or the Mice Galaxy (Barnes 2004). Seen edge-on, tidal tails appear as narrow linear structures. Finally, the simultaneous presence of two major tails on each side of NGC 680 and NGC 5557, and more in general their high fine-structure index, is totally consistent with the hypothesis that they were formed during a merger event including two spiral progenitors.

The nature of the least extended fine structures, such as the sharp-edge arclets and shells observed closer to the main bodies, is much more ambiguous. Phase wrapping of galaxy companions produces shells; radial collisions create series of interleaved ripples; the falling-back of tidal material in a major merger can generate shell-like structures as well (see Struck 1999, for a review). The analysis of the stellar populations might help us to identify the culprit. The arclet East of NGC 680 is much bluer than the surrounding material and might come from stars pulled out from a companion with different ages and metallicities. On the other hand, the shells of NGC 5557 no longer show up in the colour map of the galaxy, implying that they share the same stellar material.

4.1.3 Old versus recent, wet versus dry, mergers: how to account for the absence of a nuclear starburst?

Assuming that NGC 680 and 5557 have indeed experienced a major merger, what constraints do we have on its characteristics and age?

The fact that the tidal tails have not yet vanished gives upper limits for the merger age. The rate at with collisional material evaporates or returns to their progenitors has been quantified by Hibbard & Mihos (1995): according to their numerical simulations of the prototypical merger NGC 7252, more than 80 per cent in mass of the material located in the tails at the time of the merger will fall back within the following 2.5 Gyr. At the time of observations, 0.6 Gyr after the merger, about 3 per cent of the optical luminosity – hence of the stellar mass assuming a constant M/L ratio – emanates from the tidal tails.[3] For comparison, we estimated from the MegaCam images that the collisional debris represent about 2–4 per cent of the stellar mass of NGC 5557.[4] This relatively high value, close to that of NGC 7252, is a strong hint that the merger cannot be too old. To be conservative, an upper limit for the age of 5 Gyr may be given, corresponding to a merger occurring at a redshift below 0.5.

Furthermore, a major merger occurring at a redshift well above 0.5 would have left enough time for additional (minor) merger episodes; they would have contributed to destroy the tails. Analysing the zoom-in cosmological simulations of Martig et al. (2009), we have confirmed that even tidal tails formed in major accretion events do not seem to survive multiple collisions (Michel-Dansac et al., in preparation).

The detection of gas in the collisional debris indicates that the parent galaxies were gas-rich as well. NGC 680 contains as much as 3×10^9 M$_\odot$ of H I, a large fraction of it being distributed along the tidal tails. In the case of NGC 5557, the H I is now exclusively concentrated in star-forming objects located in the tidal tail. Their H I gas content (around 10^8 M$_\odot$) is typical for TDGs. The very presence of TDGs suggests that their host tail used to be gas-rich. Indeed, TDGs are essentially born from the collapse of gas clouds pulled out from parent merging galaxies, and not from stellar aggregates, as discussed in Section 4.2. One may then conclude that the merger responsible for the mass assembly of the galaxies under study was a gas-rich one. The claim by van Dokkum (2005) that red ETGs might be the result of recent gas-poor mergers has been challenged by Sánchez-Blázquez et al. (2009) and Serra & Oosterloo (2010). Our observations raise further doubts about it. In any case, the narrow tidal tail observed East of NGC 5557 cannot be generated in the dynamically hot progenitors that are usually considered for dry mergers. The latter produce fans and plumes rather than tails, as emphasized by Feldmann, Mayer & Carollo (2008).

The wet merger hypothesis has however some issues. During the merger a large fraction of the atomic gas is channelled on to the central regions where, transformed into molecular gas, it generally fuels a nuclear starburst though its strength and duration might depend on the geometry of the encounter (Di Matteo et al. 2008). Stellar populations with ages coincident with that of the collision are then expected in the merger remnant. However, no molecular gas has been detected in the nuclear regions of the galaxies ($M_{\rm H_2} < 10^8$ M$_\odot$) and the luminosity-weighted age of their central stars is as old as ~ 8 Gyr. In comparison, Dupraz et al. (1990) measured as much as 3.6×10^9 M$_\odot$ of H_2 in the prototypical merger NGC 7252 and the age of the star clusters located in its core was determined by Whitmore et al. (1997) to 0.6 ± 0.2 Gyr, a value in good agreement with the age estimated for the merger with numerical simulations (Hibbard & Mihos 1995).

How can these apparently contradictory pieces of information be reconciled? One hypothesis is that the parent galaxies were not so gassy, because they had lost part of their original gas due to the interaction with their environment. Alternatively, their initial gaseous disc was very extended, with an H I distribution biased towards the external regions that contribute to enrich the tidal tail but not so much the central regions.

A more likely hypothesis is that the merger is at least 1–2 Gyr old and that the merger-induced central starburst has used up all the available molecular gas. Gyr old instantaneous starbursts would have left little imprint on the stellar populations probed by optical spectrographs. In fact, following the recent work by Vega et al. (2010) who studied a sample of ETGs with the mid-IR spectrograph IRS onboard *Spitzer*, one may predict an observational signature of an ancient starburst: the emission of PAH molecules arising from carbonaceous material released by carbon stars formed at the time of the merger. No IRS spectrum exists for our targets, but in a not too distant future, the James Webb Space Telescope (JWST) should be able to check this prediction.

[3] The photometry was carried out on ESO/NTT images of the system (Belles et al., in preparation).

[4] The measure is rather tricky given the low surface brightness extension of the tidal tails. We used the detection algorithm MARSIAA (Vollmer 2011) which distributes pixels among different statistical classes, corresponding to the sky, to stars and to the LSB objects. Aperture photometry was carried out on the masks generated by MARSIAA. Further details on the method are given in Ferriere et al. (2010). Errors are mainly due to the inaccurate subtraction of the haloes of the bright stars and may reach a factor of 2 in flux.

4.1.4 The internal structural parameters: consistent with predictions for major mergers?

If NGC 680 and 5557 seem to share a common origin – a major merger that left prominent fine structures – their internal kinematics diverge. One is a fast rotator (NGC 680) and one a slow one (NGC 5557), which in the ATLAS^{3D} classification scheme makes them fundamentally different systems (Paper I). Are numerical models of major mergers able to produce objects as similar and at the same time as different as these two galaxies?

According to the analysis of the morphology and kinematics of about 100 binary merger remnants presented in Paper VI, major mergers with mass ratio 2:1 and 1:1 can form fast and slow rotators, while minor mergers of spirals only produce fast rotators. Fast rotators are naturally produced when the remnant manages to keep the initial angular momentum of the most massive companion or when the colliding galaxies have orbits that generate some angular momentum in the remnant; this is the case for prograde encounters between equal-mass spirals. This condition is relaxed if one of the colliding galaxies is a late-type spiral. This is a likely hypothesis for NGC 680, which exhibits diffuse, plume-like, tails more typical of retrograde encounters, but has at the same time a rather high gas content, suggesting that at least one of its progenitor was gas-rich and thus of a late type. On the other hand, slow rotators are formed when at least one of the merging galaxies is on a retrograde orbit with respect to the other, to cancel out the angular momentum (Jesseit et al. 2009). As noted in Paper VI, the two progenitors do not need to be on retrograde orbit; thus the long edge-sharp tidal tail observed East of NGC 5557, which is typical of prograde collisions, is still consistent with the model, provided that the second parent had a retrograde orbit. As a matter of fact, the western tidal structure is thicker, which is expected for a retrograde interaction.[5]

Another result of the simulations presented in Paper VI is that slow rotators produced by retrograde major mergers of spirals should consist of counter-rotating discs (showing thus a double σ kinematical profile; Paper II) with Kinematically Decoupled Components made of old stars in their centre. Such KDCs should be absent in fast rotators. These predictions are in agreement with the observations for NGC 680, but not for NGC 5557 which does not exhibit the expected kinematical signatures. A KDC might, however, be invisible if very small or observed with an unfavourable projection (see fig. 2 in Paper VI). It might furthermore be destroyed if the merger remnant suffers later on additional collisions. But as argued earlier, such collisions should as well contribute to wipe out the tidal tails.

Reproducing the round shape of NGC 5557 is another challenge. Unless the impact parameter is very low (Hoffman et al. 2010), binary major mergers usually produce remnants that are rather elongated. To further shape the round body of the most massive slow rotators, such as those observed in clusters of galaxies, minor accretion events following the major one might be needed (Paper VIII). Thus, the initial merger event should have occurred long ago to give enough time for these final arrangements. Modelling the metallicity and stellar populations of the putative discy progenitors, Naab & Ostriker (2009) also claimed that the merger at the origin of present-day ETGs should be at least 3–4 Gyr old. As a last possibility, the galaxy might be a rare case of nearly face-on fast rotator, with the low rotation being due to inclination. Investigating a statistically significant number of similar cases would be required to assess whether this is a sensible option.

In any case, a complex mass assembly history initiated by a major old merger followed by several minor mergers does not seem consistent with the properties of NGC 5557, as deduced from the MegaCam observations: the presence of long tidal tails argues for a $z < 0.5$ merger and no clear imprints of recently disrupted satellites, like arclets and small tails, are visible.

4.1.5 The large-scale environment: favourable to multiple mergers?

The large-scale environment impacts the mass assembly of galaxies, in particular if multiple mergers play a role.

As shown in Fig. 2, NGC 680 belongs to a rather compact group of galaxies; at least six gas-rich companions are located within a distance of 300 kpc from the galaxy. According to the Σ_3 environment density estimator (Cappellari et al. 2011b, hereafter Paper VII), which appears to correlate best with galaxy morphology, with $\Sigma_3 = 1.47\,\mathrm{Mpc}^{-2}$, NGC 680 has the densest environment explored by our survey. The closest massive galaxy lies at less than 50 kpc from its nucleus and shows evidence of a tidal interaction (see Section 3.1.1). Clearly, NGC 680 has had many opportunities to accrete gas and stellar material from several companions of various masses, though again a major merger is most likely required to form its two prominent tidal tails. In particular, the arc East of the galaxy, with its colour bluer than the surrounding stellar population, might correspond to a disrupted satellite which was recently accreted.

NGC 5557 has a lower $\Sigma_3 = 0.30\,\mathrm{Mpc}^{-2}$. It does however also belong to a group. At least 13 group members were identified in the census of van Driel et al. (2001). Their rather low velocity dispersion (about 50 km s^{-1}) favours tidal interactions and mergers. Contrary to NGC 680, NGC 5557 is by far the most massive galaxy in the group (see Fig. 1). The lack of very nearby companions and thus the low probability of further minor merger events might explain why the narrow tidal tail of NGC 5557 has survived until now, if formed in a major merger that occurred a couple of Gyr ago. The location of NGC 5557 in a moderately dense environment might, however, be relevant to explain one of its intriguing properties not well accounted for by the numerical models discussed above: its round shape. Preliminary studies indicate that the potential well of groups and clusters modify the orbits of the galaxies in such a way that collisions with a low impact parameter become more probable than in the field (Martig et al., in preparation). This contributes to enhance the merger-induced star-forming activity in interacting galaxies (Martig & Bournaud 2008) and at the same time produce rounder merger remnants (Hoffman et al. 2010).

4.2 The major merger scenario and the formation of tidal dwarf galaxies

The formation in collisional debris of objects with masses similar to that of dwarf galaxies is a by-product of major mergers. TDGs are usually observed along long tidal tails. They appear as gravitational bound gaseous and stellar systems that are kinematically decoupled from their parent galaxies. Numerical simulations are able to form them and give clues on their formation mechanism. Several formation mechanisms have been proposed: local gravitational instabilities in the stellar component (Barnes & Hernquist 1992) or gaseous component (Wetzstein, Naab & Burkert 2007), ejection of Jeans-instable gas clouds (Elmegreen, Kaufman & Thomasson

[5] Note that the two main tidal tails of merger remnants come each from one of the progenitors.

1993), a top-down scenario in which the large-scale shape of tidal forces plays a major role (Duc, Bournaud & Masset 2004), fully compressive mode of tidal forces (Renaud et al. 2009), merger of Super-Star-Clusters (Fellhauer & Kroupa 2002). The long-term survival of TDGs has also been questioned. The numerical importance of TDGs among the dwarf galaxy population will depend on their real life expectancy. The TDG candidates discovered in NGC 5557 provide useful constraints on these issues.

4.2.1 A tidal origin for the star-forming dwarfs?

The very location of the three objects along what appears as a long tidal tail from an old merger makes them natural TDG candidates. Several arguments against them being pre-existing dwarfs and thus in favour of a tidal origin are summarized here.

(i) Their velocity, as determined from the 21 cm H I line, is within 50 km s^{-1} of the systemic velocity of NGC 5557 (3219 km s^{-1}). Such a velocity difference is in the range predicted by numerical simulations of the formation of TDGs (see fig. 10 in Bournaud & Duc 2006). Furthermore, the velocity monotonically decreases along the tidal tail, consistent with expectations from streaming motions (Bournaud et al. 2004).

(ii) The dwarfs which have a uniform blue colour are hosted by a red tail likely made of an older stellar population: the $g - r$ colour of the tail is 1.3 mag redder than that of the star-forming TDG candidates. Had the tails been produced by tidally disrupted pre-existing dwarfs, their stellar populations should have been similar in the main body and tail regions. With such a hypothesis, one should as well explain why all the tidal tails from the three torn out dwarfs are perfectly aligned.

(iii) The SFR and $M_{\rm H\,I}/L_{\rm B}$ ratios of the objects are typical of evolved TDGs like those present in NGC 4694 (Duc et al. 2007).

Although there is little doubt about the tidal origin of TDG1–3-E, optical spectroscopy allowing a measure of the oxygen abundance in their H II regions might give a final answer. Indeed, TDGs are deviant objects in the mass–luminosity relation, being too metal rich for their mass (Weilbacher, Duc & Fritze-v. Alvensleben 2003). The detection of molecular gas, as traced for instance by CO, is likely given the high detection rate of TDGs (Braine et al. 2001). The lack of dark matter is finally also expected, but difficult to check with observations (Bournaud & Duc 2006).

Conversely, if these TDGs are confirmed by the independent methods described above, their discovery would be a further hint that NGC 5557 is the result of a wet major merger.

4.2.2 Long-lived TDGs: numbers and properties

As discussed earlier tidal material in mergers unavoidably falls back on to their progenitor; so do the TDGs, however at a time-scale which depends on their distance to their parent galaxies and orbital motions around their parent (Bournaud & Duc 2006). Being located at distances of at least 70 kpc from their host, the TDGs around NGC 5557 may be long-lived. What is their real age? The tail which hosts them has an estimated age of 2–5 Gyr. A recent numerical simulation of a binary merger (Bournaud, Duc & Emsellem 2008, Belles et al., in preparation) indicates that TDGs are formed very early in collisional debris. Therefore, most probably the dynamical age of the TDGs is at least 2 Gyr old. The vast majority of confirmed TDGs known so far has been identified in young, on-going, mergers. An exception is VCC 2062 in the Virgo Cluster (Duc et al. 2007). The discovery of three new (candidate) very old TDGs related here is a further proof that such second-generation objects might be long-lived and contribute to the population of satellite dwarf galaxies. Determining their exact number would be of cosmological significance.

For the lack of observations and resolution in numerical models (see though Recchi et al. 2007), the structural properties of old TDGs are ill constrained. When observed at their formation stage, they are remarkably similar to Blue Compact Dwarf Galaxies (BCDs; Duc & Mirabel 1998). Will they then evolve into dwarf Irregulars (dIrrs) if they keep their gas, be transformed into Ultra Compact Dwarf Galaxies (UCDs) – with whom they share a lack of dark matter and perhaps a similar origin in mergers (Chilingarian et al. 2011) – become gas-poor dwarf ellipticals (dEs) or even fade into dwarf Spheroidals, similar to the satellites of the Milky way, for which a tidal origin has been speculated (Metz & Kroupa 2007)? Interestingly enough, the three old TDGs near NGC 5557 plus VCC 2062 appear as still gas-rich, blue objects, with however a very low central surface brightness (unlike BCDs, dIrrs or UCDs).

For the most luminous TDG, the observed radial profile (see Fig. 13) could be fit by GALFIT with a model characterized by a Sersic index of 0.9 and an effective radius of 11 arcsec (2.1 kpc). The modelling included two components: the dwarf galaxy itself and the halo of the parent galaxy. The radial profile of TDG1-E is close to the exponential one measured in traditional dwarf elliptical galaxies. On the absolute magnitude $M_{\rm B}$ versus effective radius $R_{\rm eff}$ diagram, TDG1-E is located within the locus occupied by dEs (see fig. 1 in Misgeld & Hilker 2011), though on the high side of $R_{\rm eff}$.

The deep imaging program carried out as part of the ATLAS^{3D} and NGVS projects might contribute to identify other old, long-lived TDGs and get more statistically significant information on their properties.

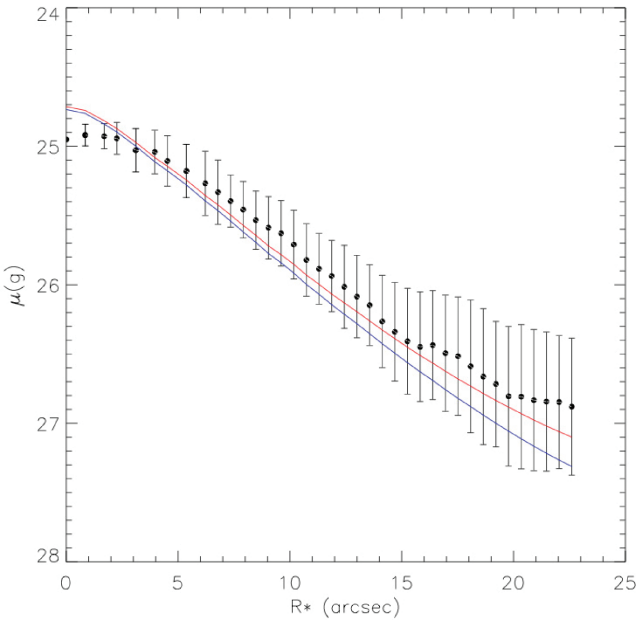

Figure 13. Surface brightness profile of TDG1-E, the most luminous TDG hosted by NGC 5557. The surface brightness in the g band (in mag arcsec^{-2}) is plotted as a function of the radius in arcsec. The black dots correspond to the observed data; the blue curve is the model profile from GALFIT with a Sersic index of 0.9; the red curve is the sum of the TDG profile and the profile of the elliptical halo in which the TDG lies.

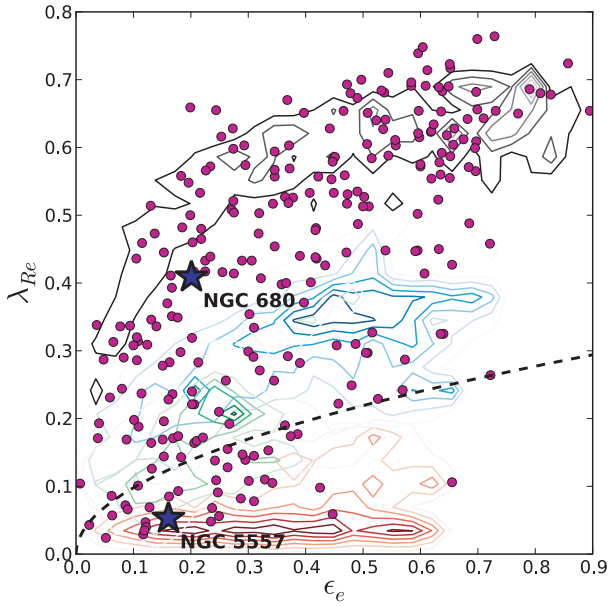

Figure 14. Position of NGC 680 and 5557 in the λ_R versus ϵ diagram. The dots represent the ATLAS^{3D} ETGs. The contours the distribution of simulated merger remnants for slow (red), fast (blue) rotators, remergers (green) and progenitors (black). Figure adapted from Paper VI.

4.3 Are NGC 680 and 5557 representative of their sub-class?

NGC 680 and 5557 are only two galaxies among the 260 of the ATLAS^{3D} sample of nearby ETGs. The question about their representativeness legitimately arises. Their location in the reference λ_R versus ϵ diagram is shown in Fig. 14, together with the other ETGs and predictions from the binary merger data base presented in Paper VI.

In many aspects, NGC 680 is typical of fast rotators, and more in general of the population of nearby ETGs. Its internal kinematics puts it in the populated class of disc rotators without KDCs (Paper II), to which 82 per cent of the ATLAS^{3D} galaxies belong. It contains atomic hydrogen, like about half of the ATLAS^{3D} ETGs outside Virgo, and its H I distribution is irregular like half of the H I-detected ETGs[6] (Serra et al., in preparation). No molecular gas was detected in this ETG like for 76 per cent of fast rotators (Paper IV).

Massive ellipticals with a round morphology like NGC 5557 are much rarer among nearby ETGs. Its kinematical group made of Non-Disc-like Rotators with no specific kinematical feature corresponds to only 5 per cent of the whole sample. Like the vast majority of slow rotators, it is not detected in CO, and H I is only found as sparse H I clouds around the galaxy.

Our observations revealed that both objects exhibit prominent gas-rich tidal tails typical of major gas-rich mergers. However, as shown in Fig. 14 and discussed earlier, simulations of single binary mergers have difficulties to reproduce simultaneously their values of λ_R and ϵ. We argue here that the binary merger model might be adequate if very specific initial conditions are considered, such as a low impact parameter for NGC 5557. Such a configuration has statistically a low probability to occur which would make NGC 5557 itself a very rare system. However, as noted in Section 4.1.4, low impact collisions may be more frequent in dense environments. In that case, NGC 5557 might be representative of slow rotators located in groups and clusters.

[6] For the other half, regular H I discs are observed.

5 SUMMARY AND CONCLUSIONS

As part of the ATLAS^{3D} project, ultra-deep MegaCam observations are currently being obtained with the CFHT for a large sample of about 100 ETGs, complementing a wealth of ancillary data on these systems, including in particular integral field optical spectroscopy, H I/CO mapping and spectroscopy. Thanks to a specific imaging strategy and dedicated data-reduction minimizing the background, detailed here, our images reach a surface brightness limit of 29 mag arcsec^{-2} in the g band. Such a sensitivity is unprecedented for field ETGs. We have presented in this paper the results obtained for two test case ellipticals. Each galaxy belongs to one of the two principal sub-classes of ETGs: the class of fast rotators, which make the bulk of nearby ETGs and the less populated class of slow rotators. Both galaxies had in common the presence of atomic hydrogen in their close vicinity.

The MegaCam images revealed optical counterparts to some previously detected intergalactic H I clouds and a number of additional fine and diffuse stellar features which were invisible on previously available optical images. The most spectacular structure is a 160-kpc long filament that sticks out from the diffuse halo of NGC 5557. It is among the longest known in the nearby Universe. The tail hosts several blue star-forming objects, detected in H I by the WSRT and in the UV by *GALEX*. They are likely TDGs born in collisional debris. Two shorter stellar tidal tails with similar morphologies as their H I counterparts are found on each side of NGC 680. More towards the central regions, a series of concentric shells and arcs are observed. In NGC 680, a few of these features might be remnants of recently disrupted satellites.

Comparing the morphology and kinematics of these structures with predictions from published numerical models of galaxy collisions, we reached the following conclusions.

(i) The tidal tails were formed during a major merger episode. Their shape, internal structure and high gas content reveal that the merger was a gas-rich one and involved progenitors with mass ratios not exceeding 1:4.

(ii) The very fact that such tidal tails are still observable, even if very faint, indicates that all the tidal material has not had the time to fall back or be dispersed by posterior accretion events and thus that the merger should have occurred at a redshift below 0.5.

(iii) The striking properties of NGC 5557 – it simultaneously exhibits a high mass, round shape, absence of KDCs, lack of significant rotation, presence of gigantic tidal tails – do not quite match those obtained with current models of ETG formation. Cosmological simulations and semi-analytic models predict that the principal mass assembly episode of massive ETGs, especially the slow rotators, is more likely to involve a wet major merger at a redshift above 1, followed by a long and complex mass accretion history.

(iv) In particular, typical binary mergers have difficulties to directly produce roundish, massive, slow rotators, unless assuming very specific initial conditions, such as a low impact parameter. We put forward the hypothesis that in rather dense environments like the group which hosts NGC 5557, collisions with a low impact parameter may indeed be favoured.

(v) Since the main body appears kinematically relaxed, the merger cannot, however, be too recent. This is further confirmed by the non-detection of molecular gas in the core of both galaxies

and absence or limited star formation activity there. Whereas NGC 680 and 5557 share many properties with the 0.6 Gyr old prototypical merger NGC 7252, in particular similar fine-structure indexes, they differ with respect to their ability to form stars. If the merger which formed them triggered a nuclear starburst, as expected for gas-rich mergers, the memory of this event has already been lost. This pushes the age of the merging episode to at least 1–2 Gyr, while the conservative upper limit provided by the mass of the tidal features still observed today may be 5 Gyr.

(vi) If the merger at the origin of NGC 5557 is indeed a couple of Gyr old, so are the gas-rich tidal dwarf galaxies discovered along its tidal tail. This would be a proof that they may survive for several Gyr.

This paper has shown the great potential of the deep imaging of galaxies to constrain their origin and indeed the in-depth analysis of NGC 680 and 5557 presented here seems to challenge the common belief on the mass assembly history of massive ellipticals. Whether these two cases are typical of ETGs, of some sub-classes of them or are rare unrepresentative objects will be addressed by our on-going MegaCam survey.

ACKNOWLEDGMENTS

We thank the referee for very useful suggestions that especially helped us in improving the readability of the figures. We are especially grateful to the CFHT team for their dedication in the queued service observing and willingness to accommodate specific modes of observation. The paper is based on observations obtained with MegaPrime/MegaCam, a joint project of CFHT and CEA/DAPNIA, at the CFHT, which is operated by the National Research Council (NRC) of Canada, the Institute National des Sciences de l'Univers of the Centre National de la Recherche Scientifique of France and the University of Hawaii. Images from the *GALEX* archives and data obtained with the WSRT, operated by the Netherlands Foundation for Research in Astronomy ASTRON, with support of NWO, have also been used. This research has made use of the NASA/IPAC Extragalactic Data base (NED) which is operated by the Jet Propulsion Laboratory, California Institute of Technology, under contract with the National Aeronautics and Space Administration. PAD, FB, EE and LMD acknowledge support from Agence Nationale de la Recherche (ANR-08-BLAN-0274-01). MC acknowledges support from a Royal Society University Research Fellowship. This work was supported by the rolling grants 'Astrophysics at Oxford' PP/E001114/1 and ST/H002456/1 and visitors grants PPA/V/S/2002/00553, PP/E001564/1 and ST/H504862/1 from the UK Research Councils. RLD acknowledges travel and computer grants from Christ Church, Oxford and support from the Royal Society in the form of a Wolfson Merit Award 502011.K502/jd. RLD also acknowledges the support of the ESO Visitor Programme which funded a 3 month stay in 2010. SK acknowledges support from the Royal Society Joint Projects Grant JP0869822. RMM is supported by the Gemini Observatory, which is operated by the Association of Universities for Research in Astronomy, Inc., on behalf of the international Gemini partnership of Argentina, Australia, Brazil, Canada, Chile, the United Kingdom and the United States of America. TN, MBois and SK acknowledge support from the DFG Cluster of Excellence 'Origin and Structure of the Universe'. MS acknowledges support from a STFC Advanced Fellowship ST/F009186/1. NS and TD acknowledge support from an STFC studentship. The authors acknowledge financial support from ESO.

REFERENCES

Barnes J. E., 2004, MNRAS, 350, 798
Barnes J. E., Hernquist L., 1992, Nat, 360, 715
Bertin E., 2006, in Gabriel C., Arviset C., Ponz D., Enrique S., eds, ASP Conf. Ser. Vol. 351. Astronomical Data Analysis Software and Systems XV. Astron. Soc. Pac., San Francisco
Bertin E., Mellier Y., Radovich M., Missonnier G., Didelon P., Morin B., 2002, in Bohlender D. A., Durand D., Handley T. H., eds, ASP Conf. Ser. Vol. 281. Astronomical Data Analysis Software and Systems XI. Astron. Soc. Pac., San Francisco
Bois M. et al., 2010, MNRAS, 406, 2405
Bois M. et al., 2011, MNRAS, 416, 1654 (Paper VI)
Bournaud F., Duc P.-A., 2006, A&A, 456, 481
Bournaud F., Duc P.-A., Amram P., Combes F., Gach J.-L., 2004, A&A, 425, 813
Bournaud F., Jog C. J., Combes F., 2007, A&A, 476, 1179
Bournaud F., Duc P.-A., Emsellem E., 2008, MNRAS, 389, L8
Braine J., Duc P.-A., Lisenfeld U., Charmandaris V., Vallejo O., Leon S., Brinks E., 2001, A&A, 378, 51
Bruzual G., Charlot S., 2003, MNRAS, 344, 1000
Burkert A., Naab T., Johansson P. H., Jesseit R., 2008, ApJ, 685, 897
Cantiello M., Blakeslee J. P., Raimondo G., Mei S., Brocato E., Capaccioli M., 2005, ApJ, 634, 239
Cappellari M. et al., 2011a, MNRAS, 413, 813 (Paper I)
Cappellari M. et al., 2011b, MNRAS, 416, 1680 (Paper VII)
Chilingarian I., Mieske S., Hilker M., Infante L., 2011, MNRAS, 412, 1627
Cimatti A. et al., 2004, Nat, 430, 184
Cortese L., Bendo G. J., Isaak K. G., Davies J. I., Kent B. R., 2010, MNRAS, 403, L26
de Zeeuw P. T. et al., 2002, MNRAS, 329, 513
Denicoló G., Terlevich R., Terlevich E., Forbes D. A., Terlevich A., 2005, MNRAS, 358, 813
Di Matteo P., Bournaud F., Martig M., Combes F., Melchior A., Semelin B., 2008, A&A, 492, 31
Di Matteo P., Jog C. J., Lehnert M. D., Combes F., Semelin B., 2009, A&A, 501, L9
Duc P.-A., Mirabel I. F., 1998, A&A, 333, 813
Duc P.-A., Bournaud F., Masset F., 2004, A&A, 427, 803
Duc P.-A., Braine J., Lisenfeld U., Brinks E., Boquien M., 2007, A&A, 475, 187
Dupraz C., Casoli F., Combes F., Kazes I., 1990, A&A, 228, L5
Ebneter K., Davis M., Djorgovski S., 1988, AJ, 95, 422
Elmegreen B. G., Kaufman M., Thomasson M., 1993, ApJ, 412, 90
Emsellem E. et al., 2011, MNRAS, 414, 888 (Paper III)
Feldmann R., Mayer L., Carollo C. M., 2008, ApJ, 684, 1062
Fellhauer M., Kroupa P., 2002, MNRAS, 330, 642
Ferriere E. et al., 2010, in Prugniel P., ed., A Universe of Dwarf Galaxies Marsiaa. Kluwer, Dordrecht
Forbes D. A., Beasley M. A., Bekki K., Brodie J. P., Strader J., 2003, Sci, 301, 1217
Gil de Paz A. et al., 2007, ApJS, 173, 185
Hibbard J. E., Mihos J. C., 1995, AJ, 110, 140
Hibbard J. E., Yun M. S., 1999, ApJ, 522, L93
Hoffman L., Cox T. J., Dutta S., Hernquist L., 2010, ApJ, 723, 818
Janowiecki S., Mihos J. C., Harding P., Feldmeier J. J., Rudick C., Morrison H., 2010, ApJ, 715, 972
Jesseit R., Cappellari M., Naab T., Emsellem E., Burkert A., 2009, MNRAS, 397, 1202
Johansson P. H., Naab T., Burkert A., 2009, ApJ, 690, 802
Johnston K. V., Bullock J. S., Sharma S., Font A., Robertson B. E., Leitner S. N., 2008, ApJ, 689, 936
Karl S. J., Naab T., Johansson P. H., Kotarba H., Boily C. M., Renaud F., Theis C., 2010, ApJ, 715, L88
Kennicutt R. C. J., 1998, ARA&A, 36, 189
Khochfar S. et al., 2011, MNRAS, in press (doi:10.1111/j.1365-2966.2011.19486.x) (Paper VIII, this issue)

Krajnović D., Emsellem E., Cappellari M., Alatalo K., Blitz L., 2011, MNRAS, 414, 2923 (Paper II)
Kuntschner H. et al., 2010, MNRAS, 408, 97
McConnachie A. W., Irwin M. J., Ibata R. A., Dubinski J., Widrow L. M., Martin N. F., Côté P., 2009, Nat, 461, 66
Magnier E. A., Cuillandre J., 2004, PASP, 116, 449
Malin D. F., Carter D., 1980, Nat, 285, 643
Martig M., Bournaud F., 2008, MNRAS, 385, L38
Martig M., Bournaud F., Teyssier R., Dekel A., 2009, ApJ, 707, 250
Martínez-Delgado D., Gómez-Flechoso M. Á., Aparicio A., Carrera R., 2004, ApJ, 601, 242
Martínez-Delgado D., Gabany R. J., Crawford K., Zibetti S., Majewski S. R., 2010, AJ, 140, 962
Metz M., Kroupa P., 2007, MNRAS, 376, 387
Michel-Dansac L. et al., 2010a, ApJ, 717, L143
Michel-Dansac L., Martig M., Bournaud F., Emsellem E., Duc P. A., Combes F., 2010b, in Debattista V. P., Popescu C. C., eds, AIP Conf. Proc. Vol. 1240, Hunting for the Dark: the Hidden Side of Galaxy Formation. Am. Inst. Phys., Melville, p. 283
Mihos J. C., Harding P., Feldmeier J., Morrison H., 2005, ApJ, 631, L41
Mirabel I. F., Lutz D., Maza J., 1991, A&A, 243, 367
Misgeld I., Hilker M., 2011, MNRAS, 414, 3699
Naab T., Ostriker J. P., 2009, ApJ, 690, 1452
Naab T., Khochfar S., Burkert A., 2006, ApJ, 636, L81
Negroponte J., White S. D. M., 1983, MNRAS, 205, 1009
O'Connell R. W., 1999, ARA&A, 37, 603
Oosterloo T. A., Morganti R., Sadler E. M., van der Hulst T., Serra P., 2007, A&A, 465, 787
Oosterloo T. et al., 2010, MNRAS, 409, 500
Paturel G., Petit C., Prugniel P., Theureau G., Rousseau J., Brouty M., Dubois P., Cambrésy L., 2003, A&A, 412, 45
Peirani S., Crockett R. M., Geen S., Khochfar S., Kaviraj S., Silk J., 2010, MNRAS, 405, 2327
Peng C. Y., Ho L. C., Impey C. D., Rix H., 2002, AJ, 124, 266
Recchi S., Theis C., Kroupa P., Hensler G., 2007, A&A, 470, L5
Regnault N. et al., 2009, A&A, 506, 999
Renaud F., Boily C. M., Naab T., Theis C., 2009, ApJ, 706, 67
Sánchez-Blázquez P., Gibson B. K., Kawata D., Cardiel N., Balcells M., 2009, MNRAS, 400, 1264
Sansom A. E., Hibbard J. E., Schweizer F., 2000, AJ, 120, 1946
Sarzi M. et al., 2010, MNRAS, 402, 2187
Sasaki S. S. et al., 2007, ApJS, 172, 511
Sault R. J., Teuben P. J., Wright M. C. H., 1995, in Shaw R. A., Payne H. E., Hayes J. J. E., eds, ASP Conf. Ser. Vol. 77, Astronomical Data Analysis Software and Systems IV. Astron. Soc. Pac., San Francisco, p. 433
Schiminovich D., van Gorkom J. H., van der Hulst J. M., Malin D. F., 1995, ApJ, 444, L77
Schweizer F., Seitzer P., 1992, AJ, 104, 1039
Schweizer F., Seitzer P., Faber S. M., Burstein D., Dalle Ore C. M., Gonzalez J. J., 1990, ApJ, 364, L33
Secker J., 1995, PASP, 107, 496
Serra P., Oosterloo T. A., 2010, MNRAS, 401, L29
Skrutskie M. F. et al., 2006, AJ, 131, 1163
Struck C., 1999, Phys. Rep., 321, 1
Tal T., van Dokkum P. G., Nelan J., Bezanson R., 2009, AJ, 138, 1417
Temi P., Brighenti F., Mathews W. G., 2007, ApJ, 660, 1215
Toomre A., 1977, in Tinsley B. M., Larson R. B., eds, Evolution of Galaxies and Stellar Populations. Yale Univ. Obser., New Haven
Tortora C., Napolitano N. R., Cardone V. F., Capaccioli M., Jetzer P., Molinaro R., 2010, MNRAS, 407, 144
van Dokkum P. G., 2005, AJ, 130, 2647
van Driel W., Marcum P., Gallagher J. S., III, Wilcots E., Guidoux C., Monnier Ragaigne D., 2001, A&A, 378, 370
van Moorsel G. A., 1988, A&A, 202, 59
Vega O. et al., 2010, ApJ, 721, 1090
Vollmer B., 2011, AJ, submitted
Weil M. L., Hernquist L., 1996, ApJ, 460, 101
Weilbacher P. M., Duc P.-A., Fritze-v.Alvensleben U., 2003, A&A, 397, 545
Wetzstein M., Naab T., Burkert A., 2007, MNRAS, 375, 805
Whitmore B. C., Miller B. W., Schweizer F., Fall S. M., 1997, AJ, 114, 1797
Witt A. N., Mandel S., Sell P. H., Dixon T., Vijh U. P., 2008, ApJ, 679, 497
Young L. M. et al., 2011, MNRAS, 414, 940 (Paper IV)

This paper has been typeset from a TEX/LATEX file prepared by the author.